

Accepted by *The Astrophysical Journal*, 2013 August 29

A Search for L/T Transition Dwarfs With Pan-STARRS1 and *WISE*: Discovery of Seven Nearby Objects Including Two Candidate Spectroscopic Variables

William M. J. Best¹, Michael C. Liu^{1,6}, Eugene A. Magnier¹, Kimberly M. Aller^{1,6}, Niall R. Deacon², Trent J. Dupuy³, Joshua Redstone⁴, W. S. Burgett¹, K. C. Chambers¹, K. W. Hodapp¹, N. Kaiser¹, R.-P. Kudritzki¹, J. S. Morgan¹, P. A. Price⁵, J. L. Tonry¹, and R. J. Wainscoat¹

ABSTRACT

We present initial results from a wide-field (30,000 deg²) search for L/T transition brown dwarfs within 25 pc using the Pan-STARRS1 and *WISE* surveys. Previous large-area searches have been incomplete for L/T transition dwarfs, because these objects are faint in optical bands and have near-infrared colors that are difficult to distinguish from background stars. To overcome these obstacles, we have cross-matched the Pan-STARRS1 (optical) and *WISE* (mid-IR) catalogs to produce a unique multi-wavelength database for finding ultracool dwarfs. As part of our initial discoveries, we have identified seven brown dwarfs in the L/T transition within 9–15 pc of the Sun. The L9.5 dwarf PSO J140.2308+45.6487 and the T1.5 dwarf PSO J307.6784+07.8263 (both independently discovered by Mace et al. 2013) show possible spectroscopic variability at the *Y*- and *J*-bands. Two more objects in our sample show evidence of photometric *J*-band variability, and two others are candidate unresolved binaries based on their spectra. We expect our full search to yield a well-defined, volume-limited sample of L/T transition dwarfs that will include many new targets for study of this complex regime. PSO J307.6784+07.8263 in particular may be an excellent candidate for in-depth study of variability, given its brightness (*J* = 14.2 mag) and proximity (11 pc).

Subject headings: brown dwarfs — stars: individual (PSO J140.2308+45.6487, PSO J307.6784+07.8236) — stars: variables: general — stars: atmospheres — binaries: general

¹Institute for Astronomy, University of Hawaii at Manoa, Honolulu, HI 96822, USA; wbest@ifa.hawaii.edu

²Max Planck Institute for Astronomy, Koenigstuhl 17, D-69117 Heidelberg, Germany

³Harvard-Smithsonian Center for Astrophysics, 60 Garden Street, Cambridge, MA 02138, USA

⁴Facebook, 335 Madison Ave, New York, NY 10017-4677, USA

⁵Department of Astrophysical Sciences, Princeton University, Princeton, NJ 08544, USA

⁶Visiting Astronomer at the Infrared Telescope Facility, which is operated by the University of Hawaii under Cooperative Agreement no. NNX-08AE38A with the National Aeronautics and Space Administration, Science Mission Directorate, Planetary Astronomy Program.

1. Introduction

Over 1,200 brown dwarfs have been cataloged since the first unambiguous discovery less than twenty years ago (Nakajima et al. 1995). As a result, two new spectral types, L and T, have been created (Kirkpatrick et al. 1999; Burgasser et al. 2006) to categorize these ultracool objects, and recent discoveries have identified the first brown dwarfs cooler than 400 K (Liu et al. 2011b; Luhman et al. 2011; Cushing et al. 2011; Kirkpatrick et al. 2012), spawning the creation of the Y spectral type. The main drivers of brown dwarf discoveries have been large-area digital surveys such as the Deep Near Infrared Survey of the Southern Sky (DENIS, Epchtein et al. 1999), the Sloan Digital Sky Survey (SDSS; York et al. 2000), the Two Micron All Sky Survey (2MASS; Skrutskie et al. 2006), and the UKIRT Infrared Deep Sky Survey (UKIDSS; Lawrence et al. 2007). Photometric searches using these surveys combined with spectroscopic follow-up have identified most of the known field brown dwarfs (e.g., Chiu et al. 2006; Cruz et al. 2007; Burningham et al. 2010). More recently, the Pan-STARRS1 3π Survey (PS1; Kaiser et al. 2010), the Wide-Field Infrared Survey Explorer (*WISE*; Wright et al. 2010), and the VISTA Hemisphere Survey (VHS; PI McMahon, Cambridge, UK) have pushed brown dwarf searches to greater distances and cooler temperatures (e.g., Deacon et al. 2011; Kirkpatrick et al. 2011; Lodieu et al. 2012).

Despite the overall success of past searches, it is expected that previous work has been less complete for L/T transition dwarfs (spectral types \approx L6–T5) because these objects are optically faint and have near-infrared colors that are difficult to distinguish from M and early-L dwarfs (e.g., Reid et al. 2008). Past searches sensitive to L/T objects have also focused on modest areas of the sky. The most successful searches so far have been those of Chiu et al. (2006), who searched over 3,500 deg² using SDSS photometry (optical *iz* bands) to find 47 L6–T5 dwarfs; Metchev et al. (2008) and Geißler et al. (2011), who cross-matched SDSS DR1 (2,099 deg²; Abazajian et al. 2003) with 2MASS (near-IR) photometry to identify 10 L6–T5 dwarfs (many of which showed spectral indications of binarity); and Day-Jones et al. (2013), who searched 495 deg² in UKIDSS and SDSS to find 15 L6–T5 dwarfs. Deacon et al. (2011, hereinafter D11) and Liu et al. (2011a; 2013, in prep) have combined Pan-STARRS1 and 2MASS photometry with proper motion to search three-quarters of the sky for T dwarfs. To date, however, there has been no large-area search specifically targeting nearby, bright L/T transition dwarfs.

Because of this slow progress in identifying the local L/T population, we do not yet have a well-constrained substellar mass function for the solar neighborhood. However, recent work indicates that the local space density has a minimum at the L/T transition (Day-Jones et al. 2013 and references therein). A natural explanation is that the L/T transition spans a fairly narrow temperature range ($\Delta T \approx 400$ K) compared to L0–L5 dwarfs ($\Delta T \approx 1000$ K; Golimowski et al. 2004; Stephens et al. 2009). Moreover, brown dwarfs cool as they age and evolve to later spectral types, resulting in a growing accumulation of late-T and Y dwarfs (Burgasser 2004). Day-Jones et al. (2013) calculate errors of $\sim 17\%$ and $\sim 40\%$ for their estimates of the space density of L7–T0.5 and T1–T4.5 dwarfs, respectively. A larger sample of L/T objects will improve these estimates, allowing more accurate assessments of the local ultracool IMF.

L/T transition dwarfs are of further interest because their spectral features indicate significant variations in surface gravity, metallicity, and/or atmospheric clouds (Kirkpatrick 2005 and references therein). In particular, many changes in these spectral features are thought to arise from the depletion of condensate clouds as brown dwarfs cool (e.g., Allard et al. 2001; Burrows et al. 2006; Saumon & Marley 2008), making L/T transition dwarfs ideal for case studies of cloud formation and gas chemistry in ultracool atmospheres. One notable example is the ~ 0.5 mag J -band brightening across the L/T transition as thick clouds dissipate to reveal lower, warmer layers of the photosphere, observed in isolated objects (Tinney et al. 2003; Dupuy & Liu 2012) as well as the components of L/T binaries (Liu et al. 2006;Looper et al. 2008).

Another likely consequence of evolving and thinning clouds is photometric variability. Optical variability is known to be common in L dwarfs (Rockenfeller et al. 2006) and is typically periodic on timescales of several hours, consistent with rotation periods of brown dwarfs (Bailer-Jones 2004; Reiners & Basri 2008). However, detection of infrared variability has proven to be much more elusive (e.g., Enoch et al. 2003; Koen et al. 2005; Goldman et al. 2008). The first unambiguous detections of near-IR photometric variability in T dwarfs were in SIMP J013656.57+093347.3 (T2.5; Artigau et al. 2009, hereinafter SIMP 0136+0933) and 2MASS J21392676+0220226 (T1.5; Radigan et al. 2012, hereinafter 2MASS 2139+0220). Notably, both of these objects are members of the L/T transition. Apai et al. (2013) have subsequently detected J - and H -band spectral variability in these objects. Buenzli et al. (2012) discovered multiband infrared sinusoidal variability in the T6.5 dwarf 2MASS 2228–4310, along with a wavelength dependence of the variability phase, indicative of vertical cloud structure. Most recently, Khandrika et al. (2013) identified photometric J -band variability in two mid-L dwarfs and K -band variability in a T8 dwarf, while also confirming the J -band variability of 2MASS 2139+0220. These observations collectively suggest that variability is a normal feature of ultracool dwarfs. Khandrika et al. (2013) estimate a variability fraction of $35\% \pm 5\%$, and surprisingly find no strong evidence of a greater frequency for L/T transition objects.

Any search for brown dwarfs, especially those in the L/T transition, must also account for binaries. L+T binaries can have colors and composite spectra that mimic those of single L/T transition dwarfs (Burgasser 2007) and can exaggerate the amplitude of the J -band brightening (Liu et al. 2006; Dupuy & Liu 2012). Components of binary systems are valuable benchmarks, as they are coeval, equidistant, and have common metallicities. They are especially valuable in the L/T transition, where they can help to set tight constraints on the observed atmospheric transitions (Dupuy et al. 2009; Liu et al. 2010). Compared to their stellar analogs, field brown dwarf binaries tend to have smaller separations (Allen et al. 2007) and mass ratios closer to unity (Allen 2007). This enables determination of their orbits and dynamical masses (e.g., Bouy et al. 2004; Liu et al. 2008; Dupuy et al. 2010; Konopacky et al. 2010), which breaks the mass/age degeneracy that plagues field brown dwarf analysis.

To increase the census of L/T transition dwarfs, we have begun a search using PS1 and *WISE*, leveraging the combined data of these optical and mid-infrared surveys. In order to construct a

well-defined sample of L/T transition dwarfs, we have limited our search to candidates within 25 parsecs of the Sun, based on their photometric distances. Several past projects, including the Gliese catalog (Gliese & Jahreiss 1995) and the PMSU M dwarf survey (Reid et al. 2002, and references therein), have searched this same volume of space for stars, so our project is well-matched to previous efforts. Our search will address a known deficiency in the solar neighborhood census, significantly improve the constraints on the local substellar mass and luminosity functions, and identify a well-defined, volume-limited sample of late L and early T dwarfs that can be used to better understand the evolution of brown dwarfs through the L/T transition.

In this paper, we present the first results of our ongoing search, namely the discovery of seven L/T transition dwarfs within 15 pc. Three objects are entirely new discoveries. The other four were identified independently by Mace et al. (2013, hereinafter M13) in their search for T dwarfs in *WISE*, though without distance estimates. (Our spectroscopic confirmation preceded the publication of M13.) We explain our search process in Section 2. We describe our observations in Section 3, and our discoveries in Section 4. We discuss the properties of specific discoveries in Section 5, and summarize our findings in Section 6.

2. Search Method

We identified candidate L/T dwarfs through a series of quality, color, and magnitude cuts applied to our merged PS1+*WISE* database, followed by visual inspection of PS1, 2MASS, and *WISE* images. We then obtained and typed spectra of candidates using standard procedures described in Section 3.

The PS1 3π survey (Chambers et al., in prep) is obtaining multi-epoch imaging in five optical bands ($g_{P1}, r_{P1}, i_{P1}, z_{P1}, y_{P1}$) with a 1.8-meter wide-field telescope on Haleakala, Maui, covering the entire sky north of declination -30° . Images are processed nightly through the Image Processing Pipeline (IPP; Magnier 2006, 2007; Magnier et al. 2008), with photometry on the AB magnitude scale (Tonry et al. 2012). Imaging began in May 2010 and should be completed by early 2014. The *WISE* All-Sky Release includes data taken between January and August 2010 (Cutri et al. 2012) in four mid-infrared bands: *W1* ($3.6 \mu\text{m}$), *W2* ($4.5 \mu\text{m}$), *W3* ($12 \mu\text{m}$), and *W4* ($22 \mu\text{m}$). We merged all PS1 detections through January 2012 with the *WISE* All-Sky catalog using a $3.0''$ matching radius. Because the two surveys are nearly contemporaneous, matching by position is effective for all but the highest proper motion objects. Matching the two surveys by position also eliminates transient objects (e.g., asteroids) in regions the surveys have only covered once. Candidates were selected from the full three-quarters of sky covered by the merged database.

To extract candidate L/T transition dwarfs from our PS1+*WISE* database, we applied the following quality-of-detection criteria (items shown in parentheses refer to flags within the database):

1. Detected in at least two separate y_{P1} frames ($y:nphot \geq 2$), to reject transients.

2. $\sigma_y < 0.2$ mag (`y:err < 0.2`), establishing $S/N > 5$ as the detection threshold for y_{P1} .
3. “Good” or “poor” quality y_{P1} photometry, but not “bad”, as defined in the PS1 DVO database (`y:flags = 256` or `y:flags = 512`), i.e., clear PSF identification, no saturated objects or cosmic rays.
4. $W1$ and $W2$ detections have $S/N > 2$ (`ph_qual = A, B, or C`).
5. $W1$ and $W2$ detections are not saturated (`w1sat = 0` and `w2sat = 0`).
6. $W1$ and $W2$ detections are point sources (`ext_flg = 0`).
7. $W1$ and $W2$ detections are unlikely to be variable (`var_flg ≤ 4`).

We thus required that candidates have good detections in y_{P1} , $W1$, and $W2$, but not necessarily in any other bands. We then applied the following color criteria, which are illustrated by Figures 1–3:

1. No more than one total detection in either g_{P1} or r_{P1} (`g:nphot + r:nphot < 2`), unless each band had only a single detection with $\sigma > 0.2$ mag. Among known L/T transition dwarfs, none are detected in g_{P1} and only one in r_{P1} — the nearby, unusually blue L6 dwarf SDSS J1416+1348 (Bowler et al. 2010). We therefore expect previously undiscovered L/T transition dwarfs to be too red to show up in g_{P1} and r_{P1} and this criterion rejects objects that are clearly detected in these bluer bands.
2. $i_{P1} - z_{P1} \geq 1.8$ mag (Figure 1), to exclude objects of spectral type mid-L and earlier. We applied this criterion only when the i_{P1} and z_{P1} photometry for an object met the same quality standards required for y_{P1} detections, i.e., $\sigma_i < 0.2$ mag and $\sigma_z < 0.2$ mag (`i:err < 0.2` and `z:err < 0.2`) with at least two detections in both i_{P1} and z_{P1} (`i:nphot ≥ 2` and `z:nphot ≥ 2`, to reject transient detections). Of the L/T transition dwarfs too faint to have been previously discovered in 2MASS and SDSS, even the brightest are likely to be near the detection limits of i_{P1} and z_{P1} . (In fact, we do not detect any known T dwarfs in i_{P1} .) So we only applied this cut when we had good quality photometry in both bands, and accepted objects with marginal or null detections in i_{P1} and z_{P1} as long as they passed the other cuts. We note that this criterion is somewhat more relaxed than the $i - z > 2.2$ mag and $\sigma_z < 0.12$ mag cuts used by Chiu et al. (2006) in their SDSS brown dwarf search.
3. $i_{P1} - y_{P1} \geq 2.8$ mag (Figure 1), also to exclude objects of spectral type mid-L and earlier. Again, we only applied this criterion if the i_{P1} photometry for an object met the same quality standards required for y_{P1} detections, i.e., $\sigma_i < 0.2$ mag (`i:err < 0.2`) and detection in i_{P1} in at least two separate frames (`i:nphot ≥ 2`).
4. $z_{P1} - y_{P1} \geq 0.6$ mag (Figure 2), to screen out early-M dwarfs. Similarly to the $i_{P1} - z_{P1}$ and $i_{P1} - y_{P1}$ cuts, we only applied this cut if the z_{P1} photometry for an object met the same quality standards required for y_{P1} detections, i.e., $\sigma_z < 0.2$ mag (`z:err < 0.2`) and detection

in z_{P1} in at least two separate frames ($z:nphot \geq 2$). This cut was also used by D11 in their PS1+2MASS T dwarf search.

5. $y_{P1} - W1 \geq 3.0$ mag (Figure 3), to screen out early- and mid-M dwarfs. We expect this cut will have also rejected some late T dwarfs ($SpT \gtrsim T6$), which have bluer $y_{P1} - W1$ colors than L/T transition dwarfs.
6. $W1 - W2 \geq 0.4$ mag (Figure 3), to remove as many M and early-L dwarfs as possible. Kirkpatrick et al. (2011) and M13 used this same cut in their *WISE* search for nearby L and T dwarfs, but also restricted their search to bright objects with no 2MASS counterpart (i.e., objects which had moved more than 3" between 2MASS and *WISE*), criteria that we do not use here. Liu et al. (2011a) used a redder $W1 - W2 > 0.7$ mag cut to search only for T dwarfs.
7. $W2 - W3 \leq 2.5$ mag (Figure 2), to screen out extragalactic sources, as suggested by Figure 12 of Wright et al. (2010). Many of our candidates were not actually detected in *W3*, but *WISE* reports a lower magnitude limit for all non-detections, so we used the $W2 - W3$ value as an upper limit in those cases. Kirkpatrick et al. (2011) and M13 used $W1 - W2 > 0.96(W2 - W3) - 0.96$ mag for this purpose.

We then applied cuts based on spatial position:

1. We rejected all candidates within 3° of the Galactic plane.
2. To avoid objects in reddened star forming regions, we inspected the (RA, Dec) positions of candidates within 20° of the Galactic plane and rejected those that were clumped in tight groups.
3. We further rejected all remaining candidates in the highly reddened regions identified by Cruz et al. (2003), unless a candidate had a proper motion measured with $S/N > 3$ (based on 2MASS and PS1 astrometry).

We then reviewed the available images for each remaining candidate in all five PS1 filters (g , r , i , z , y), all three 2MASS filters (J , H , K), and *WISE* $W1$, $W2$, and $W3$. We rejected objects that were clearly artifacts (e.g., diffraction spikes or halos) in one or more bands or non-point sources such as galaxies.

As a final filter, we required objects to have sufficiently red $y - J$ colors to be in the L/T transition. We cross-matched our candidate list with the 2MASS, UKIDSS DR8 (Hambly et al. 2008; Lawrence et al. 2012), and VISTA DR1 (Cross et al. 2012) catalogs, and used J magnitudes from those catalogs when available with $\sigma_J < 0.1$ mag. The UKIDSS photometric system uses MKO standards (Tokunaga et al. 2002) and is described in Hewett et al. (2006). The VISTA filters are similar to those of UKIDSS, except that VISTA uses a K_s filter similar to that of 2MASS

(Lodieu et al. 2012)¹. (A precise calibration of the VISTA photometric system has not yet been published.) For objects not found in any of these catalogs, we obtained our own photometry with UKIRT/WFCAM on the MKO system (as described in Section 3). We selected objects with $y_{P1} - J_{2MASS} \geq 1.8$ mag (Figure 4) or $y_{P1} - J_{MKO} \geq 1.9$ mag, removing bluer objects that were likely to be late-M and early-L dwarfs from our candidate list. This cut does permit objects bluer than the $2.2 < y_{P1} - J_{2MASS} < 5.0$ mag cut used by D11, who searched exclusively for T dwarfs. Unlike D11, we did not apply a $J - H$ cut to our sample.

Because of the spectral changes endemic to L/T objects, y_{P1} absolute magnitudes are almost flat across the transition, from about L8 to T3 spectral types. Therefore, choosing a y_{P1} -magnitude limit approximately creates a volume-limited sample, with only modest contamination by intrinsically brighter objects that lie beyond the search radius. For follow-up observations, we chose candidates with $y_{P1} < 19.3$ mag to search the solar neighborhood for single L/T objects out to 25 pc, acknowledging that our search will also detect unresolved binaries out to larger distances.

3. Observations

We obtained follow-up near-IR imaging of our candidates using WFCAM (Casali et al. 2007) on the United Kingdom InfraRed Telescope (UKIRT) in queue mode. Over five nights spanning 2012 September 19–21 and 2012 December 13–14 UT, we observed a total of 308 candidates in different combinations of the Y , J , H and K bands (MKO system). Conditions were generally clear with seeing $\approx 0.6''$ on the September nights, while the December nights had many high clouds with seeing $\approx 0.8''$. Data were reduced and calibrated at the Cambridge Astronomical Survey Unit using the WFCAM survey pipeline (Irwin et al. 2004; Hodgkin et al. 2009).

We obtained low resolution near-IR spectra for our seven discoveries over eight nights in 2012 September, October and November and 2013 January with the NASA Infrared Telescope Facility (IRTF). We obtained additional spectra for PSO J307.6784+07.8263 (hereinafter PSO J307.6+07) on 2013 April 3–5, contemporaneously with the nearby M1V star 2MASS J20410101+0014278 (West et al. 2011, hereinafter 2MASS J2041+0014) for comparison. We used the facility spectrograph SpeX (Rayner et al. 2003) in prism ($R \sim 100$) and SXD ($R \sim 750$) modes with the $0.5''$ and $0.8''$ slits. Details of our observations are listed in Table 1. We observed a nearby A0V star contemporaneously with each science target for telluric calibration. All spectra were reduced using version 3.4 of the Spxtool software package (Vacca et al. 2003; Cushing et al. 2004).

Initial spectral typing of candidates was accomplished using spectral indices from Burgasser et al. (2006), with spectral types assigned using the polynomial fits from Burgasser (2007). The spectra were then visually compared to near-infrared spectra for L dwarf (Kirkpatrick et al. 2010) and T dwarf spectral standards (Burgasser et al. 2006) for final assignment of spectral types.

¹For VISTA bandpass information, see <http://casu.ast.cam.ac.uk/surveys-projects/vista/technical/filter-set>.

Following the procedure of Kirkpatrick et al. (2010), when comparing our candidate spectra with L dwarf standards, we first compared only the $0.9 - 1.4 \mu\text{m}$ portions of the spectra to evaluate the goodness of fit. If the best match for a candidate was determined to be an L dwarf standard, then we compared the candidate spectrum to that of the standard over $1.4 - 2.4 \mu\text{m}$ to determine if the candidate was unusually red or blue for its spectral type. When comparing candidates to T dwarf standards, we judged the goodness of fit for the entire $0.9 - 2.4 \mu\text{m}$ window simultaneously.

4. Results

We present here seven bright initial L/T transition discoveries from our ongoing search. Our photometric distances place all seven within $9 - 15 \text{ pc}$ of the Sun, assuming they are single objects and not unresolved binaries. The astrometric, photometric, and spectral properties of these objects are listed in Tables 2 and 3. Near-IR SpeX prism spectra for these objects are shown in Figure 5.

Four of our seven new objects have been announced by M13 in their search for late-T and Y dwarfs in *WISE*; our discovery of all four was independent (our spectroscopic confirmation preceded publication of their paper). For the most part, we agree with the spectral indices and types published by M13, and we present additional photometry, photometric distances, astrometry, and spectral indices for the four objects, as well as higher-resolution SXD spectra for two of them. Specific objects are discussed in Section 5.

We used the *W2* absolute magnitude vs. spectral type polynomial from Dupuy & Liu (2012)² to calculate photometric distances. The *W2* polynomial was determined using objects of spectral types M5.5 to T9 and has an rms scatter about the fit of 0.35 mag (slightly lower than the rms scatter of 0.39 mag for the *W1* polynomial). However, the scatter about the fit is smaller for later spectral types than for M dwarfs. Liu et al. (2011a) calculated an rms scatter of 0.18 mag for a *W2* polynomial relationship using only objects with spectral types L5 and later. We adopted this rms to determine the uncertainty in the distance.

We combined 2MASS and PS1 astrometry to calculate proper motions for our discoveries and used our photometric distances to estimate tangential velocities. A comparison of these v_{tan} estimates to the $\sigma_{v_{tan}}$ vs. v_{tan} relations in Dupuy & Liu (2012, Figure 31) indicates that all seven discoveries are very likely to be members of the thin disk.

Figures 1–4 display i_{P1} through *W3* colors of known ultracool dwarfs³, overlaid with our seven discoveries. Compared with other early-T dwarfs, PSO J307.6+07 (T1.5) is unusually blue in

²Updated polynomials can be found in the Database of Ultracool Parallaxes maintained by Trent Dupuy at https://www.cfa.harvard.edu/~tdupuy/plx/Database_of_Ultracool_Parallaxes.html. Here we use the version posted on 2012 June 09.

³Compiled from DwarfArchives.org as of April 2011, Leggett et al. (2010), Burgasser et al. (2011), and Gelino et al. (2011).

$y_{P1} - W1$ (by ~ 0.7 mag) and $y_{P1} - J_{2\text{MASS}}$ (by ~ 0.3 mag), suggesting that its y_{P1} flux is unusually bright. In addition, the six objects that have spectral types L9–T1.5 are all bluer than typical late-L and early-T dwarfs by about half a magnitude in $y_{P1} - J_{2\text{MASS}}$. We find no systematic reason why our search method would preferentially discover objects that are bluer in $y_{P1} - J_{2\text{MASS}}$. It is possible that the previous searches that identified the known objects were biased toward finding objects with redder $y_{P1} - J_{2\text{MASS}}$ colors (e.g., D11).

5. Discussion

5.1. Candidate Spectroscopic Variables

PSO J140.2308+45.6487 (hereinafter PSO J140.2+45), also known as WISE 0920+4538, and PSO J307.6+07, also known as WISE J2030+0749, are the second and third L/T transition dwarfs to be identified as candidate near-IR variables via spectroscopy, following SDSS J125453.90–012247.4 (Goldman et al. 2008). Spectra of PSO J140.2+45 taken on two different nights (Figure 6) show small but clear differences in the Y - and J -bands, while for PSO J307.6+07 (Figure 7) the difference in J -band is readily apparent. For comparison, Figure 8 shows SXD and prism spectra for PSO J339.0734+51.0978 (hereinafter PSO J339.0+51) taken ten nights apart with no clear variability.

For all three of these objects, we have normalized the pairs of spectra to the H -band peak ($1.58 \mu\text{m}$). These spectra are not absolutely calibrated, so we cannot determine with certainty the absolute changes in flux in each band; however, we note that each object’s H - and K -bands show no significant change in spectral shape or in flux relative to the adjacent absorption bands. We calculated the differences in flux in the Y - and J -bands for each pair of spectra by first convolving our spectra in the wavelength intervals $0.95 - 1.13 \mu\text{m}$ and $1.16 - 1.33 \mu\text{m}$ with the UKIDSS Y ($0.97 - 1.07 \mu\text{m}$, Hewett et al. 2006) and J ($1.17 - 1.33 \mu\text{m}$, Tokunaga et al. 2002) filter profiles, respectively. We then integrated the convolved spectra over each interval, subtracted to get the differences in flux, and converted these flux differences and their uncertainties to magnitudes. In addition, we calculated the differences in magnitude in the narrow peaks of the Y -band ($1.06 - 1.10 \mu\text{m}$) and J -band ($1.27 - 1.30 \mu\text{m}$) using the same method.

Details of each candidate variable are described below; here we discuss briefly the possible causes of variability. Artigau et al. (2009) and Radigan et al. (2012) explain the J -band photometric variations in the early-T dwarfs SIMP 0136+0933 and 2MASS 2139+0220 as consequences of the clearing of atmospheric condensate clouds, the process thought to cause the observed J -band brightening in the L/T transition. The variations are seen only in the J -band because the condensates in question are primarily silicates that absorb most strongly at J -band wavelengths compared to other (gaseous) opacity sources (Ackerman & Marley 2001; Burrows et al. 2006). The clearing process is not well understood. Several scenarios have been proposed wherein condensate clouds thin gradually (reducing their opacities), rain out suddenly, or break up (e.g., Ackerman & Marley

2001; Knapp et al. 2004; Tsuji 2005; Burrows et al. 2006; Marley et al. 2010). Models using a mixture of thin and thick clouds may generate a better match to observed early-T dwarf spectra (Buenzli et al. 2012). Radigan et al. (2012) attempt a variety of model atmosphere fits to their observations of 2MASS 2139+0220 and find success combining models with different condensate sedimentation efficiencies, interpreted as heterogenous cloud formations. J -band variation over a period of several days could therefore be a sign of thinner and thicker clouds or even breaks in clouds, changing due to rotation and/or convective processes.

5.1.1. *PSO J140.2308+45.6487 (WISE 092055.40+453856.3)*

PSO J140.2+45 was first identified photometrically as a candidate L4–L5 brown dwarf (WISE 0920+4538) by Aberasturi et al. (2011) based on *WISE*/2MASS/SDSS photometry and measurable proper motion. Our spectra of PSO J140.2+45 taken two and a half months apart (Figure 6) indicate a marginal decrease of 0.05 ± 0.04 mag in the full Y -band, but a significant decrease of 0.14 ± 0.03 mag in the Y -band peak. The decrease in J -band is also marginal: 0.05 ± 0.02 mag in the full band, and 0.03 ± 0.02 mag in the J -band peak. Visual classification of our SpeX spectrum for PSO J140.2+45 gives a spectral type L9.5, consistent with the L9.6 spectral type derived from the spectral indices. M13 classify this object as L9 and a weak binary candidate. Further observations are needed to confirm the near-IR variability of this object.

5.1.2. *PSO J307.6784+07.8263 (WISE 203042.79+074934.7)*

Figure 9 compares our SXD spectrum for PSO J307.6+07 with that of the T2 standard SDSS 1254–0122 (Leggett et al. 2000; Cushing et al. 2005; Burgasser et al. 2006). No unusual spectral features are apparent in PSO J307.6+07 at this resolution ($R \sim 750$). The spectrum of PSO J307.6+07 is reasonably close to that of SDSS 1254–0122 but has slightly weaker methane absorption at $\sim 1.15 \mu\text{m}$. The spectral indices have a mean classification of $T0.9 \pm 1.3$. Given these estimates, we classify PSO J307.6+07 as a T1.5 dwarf. M13 identified this object as WISE 2030+0749 and assigned it the same spectral type.

Our spectra of PSO J307.6+07 taken six nights apart in 2012 September (Figure 7) show a decrease of 0.11 ± 0.02 mag in the full J -band, and 0.10 ± 0.02 mag in the J -band peak. The overlaid spectra also suggest an increase in the Y -band flux over the six-night span, but we calculate this difference as only 0.02 ± 0.06 mag in the full Y -band, and 0.02 ± 0.05 mag in the Y -band peak.

Figure 10 shows spectra of PSO J307.6+07 obtained on three consecutive nights in 2013 April, along with the two 2012 September spectra from Figure 7. When examining the spectra of the comparison M1V star 2MASS J2041+0014 (presumably a non-variable source) from the same three April nights, we noticed a dimming at wavelengths $\lesssim 1.3 \mu\text{m}$ on April 3 compared to the two subsequent nights. This dimming may be due to the presence of a crescent Moon about 6° from

the standard star during this night’s observations. To correct for the dimming, we divided the April 4 spectrum of 2MASS J2041+0014 by its April 3 spectrum, and then multiplied this quotient into the April 3 spectrum of PSO J307.6+07. With this correction applied, the April data for PSO J307.6+07 show essentially no variation over the three nights. In the J -band, the April spectra also match well the 2012 September 20 spectrum, with only the September 26th SXD spectrum showing a clear difference in flux. However, in the Y -band, the April spectra all have noticeably lower flux than both of the September spectra.

Collectively, our data show significant spectroscopic variation for PSO J307.6+07 in 2012 September, and no variation in 2013 April. The reason for this apparent contradiction is unclear. The long-term stability of near-IR spectroscopic variations in L/T transition dwarfs is not well understood, so it is possible that the 2012 September observations simply occurred during an epoch of variability for PSO J307.6+07, while the 2013 April observations found the object in an epoch of constancy (or diminished variability). It is also possible that the detected variability is a result of an unrecognized oversight in the observations or data reduction. We note that the April data were obtained at higher airmass; care was taken during these observations to ensure the instrument slit was aligned with the parallactic angle, and the standard stars were observed at similar airmasses (within 0.1). We note as well that the September 26th spectrum is the only one obtained in SXD (cross-dispersed) mode. We have stitched the different orders together using the standard Spextool procedure *xcombspec* to create a single spectrum, and it is possible that this procedure has scaled one or more orders to an incorrect flux. We consider this to be unlikely for three reasons: Cushing et al. (2005) showed that order stitching with *xcombspec* results in a mean color difference of $\langle \delta_{J-H} \rangle = 0.00 \pm 0.04$ mag, much smaller than the ΔJ we detected in PSO J307.6+07; we used the same stitching procedure to obtain the spectrum for PSO J339.0+51 (Figure 8), in which we find no significant variation; and we see similar spectral variation in PSO J140.2+45, where both spectra were obtained in prism mode. Overall, we cannot establish a decisive reason for the difference of the intra-night behavior between our 2012 Sept and 2013 April datasets, so we label PSO J307.6+07 a candidate spectroscopic variable. Further observations on multiple nights are needed to confirm or reject this object as a near-IR variable.

5.2. Candidate Photometric Variables

Since our seven discoveries are bright, they are all well detected in 2MASS. We can compare our MKO photometry to the 2MASS measurements as a simple two-epoch check for near-IR variability over a period of approximately ten years. (Note that we do not use our SpeX data to synthesize the conversions directly for each object, because the spectra and photometry were all obtained at different epochs.) We used the polynomial relations of Stephens & Leggett (2004, Table 4) to bring the two epochs of JHK photometry onto a common system. The UKIRT/WFCAM JHK filters were designed on the MKO photometric system, so we converted the 2MASS photometry for our discoveries to MKO. We find that the 2MASS and MKO JHK magnitudes of our objects are

consistent within 0.1 mag, with two exceptions described below.

5.2.1. PSO J272.4689–04.8036 (WISE 180952.53–044812.5)

We assign a spectral type of T1 to PSO J272.4689–04.8036 (hereinafter PSO 272.4–04), although it is fainter in the H -band than the T1 standard SDSS J0151+1244 (Geballe et al. 2002; Burgasser et al. 2006). M13 classify this object as a T0.5 (WISE 1809–0448). Its J_{MKO} magnitude, as converted from its 2MASS photometry, is 14.94 ± 0.06 mag, about 0.2 mag brighter than our UKIRT measurement of $J_{\text{MKO}} = 15.15 \pm 0.01$ mag, a sign of potential J -band variability. The $K_{\text{MKO}} = 13.99 \pm 0.06$ mag (converted from 2MASS) and VISTA $K_{\text{MKO}} = 13.98 \pm 0.01$ mag measurements are consistent.

5.2.2. PSO J339.0734+51.0978 (WISE 223617.59+510551.9)

We find PSO J339.0734+51.0978 (hereinafter PSO J339.0+51) to be a good match to the T5 standard 2MASS J1503+2525 (Burgasser et al. 2003, 2006). Analysis of spectral indices gives a mean spectral type of $T5.1 \pm 0.1$, so we assign a spectral type of T5, a half-type earlier than the T5.5 (WISE 2236+5105) assigned by M13. The J_{MKO} magnitude, converted from 2MASS, is 14.31 ± 0.04 mag, about 0.15 mag brighter than the UKIRT $J_{\text{MKO}} = 14.46 \pm 0.01$ mag, so this object is another potential J -band variable. The H -band magnitudes of $H_{\text{MKO}} = 14.53 \pm 0.05$ mag (converted from 2MASS) and UKIRT $H_{\text{MKO}} = 14.62 \pm 0.02$ mag are consistent within 2σ . We do not have K_{MKO} photometry for PSO J339.0+51. We note that this object does not show any difference in spectra taken ten nights apart (Figure 8).

5.3. Candidate Binaries

We have examined our seven discoveries for unusual spectral features that might suggest unresolved binarity, by comparing their spectral indices to the index-index and index-spectral type plots in Burgasser et al. (2010, hereinafter B10). We found evidence for binarity in two of our discoveries, described individually below. We performed spectral decomposition analysis on these two objects following the method described in Section 5.2 of Dupuy & Liu (2012). Briefly, we used the library of 178 IRTF/SpeX prism spectra presented in B10 to create summed spectra. For each template pairing we determined the scale factors needed to minimize the χ^2 of the difference with our observed spectrum. We then examined the resulting best pairing to determine the component spectral types, taking into account factors such as larger than average spectral type uncertainties in the best-match templates and the full range of properties implied when there were multiple matches giving equally good fits. We estimated the flux ratios in standard near-infrared bandpasses using our χ^2 values and the weighting scheme described in Burgasser et al. (2010). Our derived

component spectral types and their corresponding uncertainties are listed in Table 4, and the best template pairing for each binary is shown in Figure 11. (Our analysis does not assess whether binary templates are better matches to our observed spectra than single-object templates.) For these template pairs, we calculate photometric distances by convolving absolute magnitudes for each component spectral type, determined using the same method as in Section 4.

5.3.1. *PSO J103.0927+41.4601*

Visually, the spectrum of PSO J103.0927+41.4601 (hereinafter PSO J103.0+41) appears to be a slightly earlier spectral type than the T0 standard SDSS J1207+0244 (Knapp et al. 2004; Burgasser et al. 2006). The spectral indices, however, indicate a spectral type of T0.5 for PSO J103.0+41. Assuming this is a single object, we settle on a classification of T0, placing the object at a photometric distance of 14.2 ± 1.2 pc. However, the closest spectral match is in fact the L6+T2 binary SDSS 0423–0414AB (Geballe et al. 2002; Burgasser et al. 2005; Dupuy & Liu 2012), and we find excellent agreement with a template pairing of L8+T2.5 (Figure 11, Table 4), which would indicate a distance of 20.1 ± 2.4 pc. PSO J103.0+41 also lies on the border of the binary regions in three of the B10 index-index plots. This object is therefore an appealing candidate for high-resolution imaging.

5.3.2. *PSO J282.7576+59.5858*

PSO J282.7576+59.5858 (hereinafter PSO J282.7+59) is not a good match to any of the T dwarf spectral standards. Its spectral indices average to L8.5, and our best visual *J*-band fit is L9, but the *H*- and *K*-band peaks have lower flux than the L9 standard 2MASS J0255–4700 (Martín et al. 1999; Kirkpatrick et al. 2010). The shape of the *H*-band peak is almost flat with a slight increase toward longer wavelengths, a feature more typical of early L-dwarfs (see Figure 10 in Kirkpatrick et al. 2010). We tentatively classify PSO J282.7+59 as an L9 for a single object (photometric distance 13.0 ± 1.1 pc), but the discordance in its spectral features suggests that we are looking at a blended spectrum. The best spectral match among known ultracool dwarfs is actually the suspected triple system DENIS-P 0205–1159 (Bouy et al. 2005). The spectral indices of PSO J282.7+59 do not place it in any of the binary regions of the B10 index-index plots, but B10 noted that their selection process was probably biased against systems with more than two components. We find the best match for binaries has a template pairing of L7+T4.5 (Figure 11, Table 4), at a distance of 17.9 ± 2.1 pc.

5.4. Our Discoveries in Other Surveys

All seven of the newly discovered objects are brighter than most known L/T transition dwarfs. This raises the question of why the objects were not discovered earlier. One reason is that several of the major surveys used in previous brown dwarf searches covered smaller fractions of the sky than PS1. Of our seven objects, only two are in regions covered by SDSS (PSO J103.0+41 and PSO J142.2+45) and only two lie within the UKIDSS search area (PSO J007.7921+57.8267 and PSO J142.2+45 again). Another reason is that we have searched close to the Galactic plane, using proper motion as well as colors to distinguish brown dwarf candidates from reddened background objects. Three of our seven discoveries have $|b| < 10^\circ$, putting them in crowded regions commonly avoided in previous searches (e.g., Burgasser et al. 2004). Our combination of y_{P1} and *WISE* photometry has also enabled us to discover objects whose *JHK* colors were excluded in near-infrared searches (e.g., Cruz et al. 2003).

6. Summary

We have discovered seven L/T transition dwarfs within 9 – 15 pc of the Sun based on a search of the combined Pan-STARRS1 3π and *WISE* databases. We highlight several specific objects:

- PSO J140.2+45 (L9.5) and PSO J307.6+07 (T1.5) show changes in their *J*-band spectra taken on different nights. PSO J140.2+45 also shows a marginal change in *Y*-band flux. If confirmed by subsequent observations, these would be the third and fourth known near-infrared L/T transition variables, and PSO J307.6+07 would be the second brightest, following SIMP 0136+0933. PSO J307.6+07 also has unusually blue $y_{P1} - W1$ and $y_{P1} - J$ colors compared to previously known objects of similar spectral type.
- PSO J272.4–04 (T1) and PSO J339.0+51 (T5) have inconsistent 2MASS and UKIRT *J* magnitudes (by 0.2 and 0.15 mag, respectively), possibly signs of *J*-band variability.
- PSO J103.0+41 (T0) and PSO J282.7+59 (L9) show spectral evidence that they are not single objects, including similarity to previously known multiple systems. High resolution spatial and spectroscopic observations are needed to investigate the possible multiplicity of these objects.

These brown dwarfs are all relatively bright ($J < 15.5$) and easily close enough for accurate parallax measurements. All seven are excellent targets for observations studying the atmospheric processes endemic to the L/T transition.

We thank the referee for helpful comments that improved the quality of this paper. The Pan-STARRS1 Surveys (PS1) have been made possible through contributions of the Institute for Astronomy, the University of Hawaii, the Pan-STARRS Project Office, the Max Planck Society and

its participating institutes, the Max Planck Institute for Astronomy, Heidelberg and the Max Planck Institute for Extraterrestrial Physics, Garching, The Johns Hopkins University, the University of Durham, the University of Edinburgh, Queens University Belfast, the Harvard-Smithsonian Center for Astrophysics, the Las Cumbres Observatory Global Telescope Network, Inc., the National Central University of Taiwan, the Space Telescope Science Institute, the National Aeronautics and Space Administration under Grant No. NNX08AR22G issued through the Planetary Science Division of the NASA Science Mission Directorate, and the University of Maryland. We thank the PS1 observing and processing staff for obtaining the PS1 data, and Bill Sweeney, Heather Flewelling, and Mark Huber for assistance with accessing PS1 images. The United Kingdom Infrared Telescope is operated by the Joint Astronomy Centre on behalf of the Science and Technology Facilities Council of the U.K. This paper makes use of observations processed by the Cambridge Astronomy Survey Unit (CASU) at the Institute of Astronomy, University of Cambridge. We thank Mike Irwin, Simon Hodgkin, and the team at CASU for making the reduced WFCAM data available promptly, and Watson Varricatt and the UKIRT staff for carrying out our observations. We also thank John Rayner and Alan Tokunaga for making engineering time available for IRTF observations, and Katelyn Allers, Michael Kotson, Brian Cabreira, Bill Golisch, Dave Griep, and Eric Volqardsen for assisting with these. This project makes use of data products from the Wide-field Infrared Survey Explorer, which is a joint project of the University of California, Los Angeles, and the Jet Propulsion Laboratory/California Institute of Technology, funded by the National Aeronautics and Space Administration. This research has made use of the 2MASS data products; the UKIDSS data products; the VISTA data products; NASA’s Astrophysical Data System; the SIMBAD database operated at CDS, Strasbourg, France, the SpeX Prism Spectral Libraries, maintained by Adam Burgasser at <http://pono.ucsd.edu/~adam/browndwarfs/spexprism>, and the Database of Ultracool Parallaxes, maintained by Trent Dupuy at <https://www.cfa.harvard.edu/~tdupuy/plx>. WMJB is supported by NSF grant AST09-09222. Finally, the authors wish to recognize and acknowledge the very significant cultural role and reverence that the summit of Mauna Kea has always held within the indigenous Hawaiian community. We are most fortunate to have the opportunity to conduct observations from this mountain.

Facilities: IRTF (SpeX), PS1, UKIRT (WFCAM)

REFERENCES

- Abazajian, K., Adelman-McCarthy, J. K., Agüeros, M. A., et al. 2003, *AJ*, 126, 2081
- Aberasturi, M., Solano, E., & Martin, E. L. 2011, *A&A*, 534, L7
- Ackerman, A. S., & Marley, M. S. 2001, *ApJ*, 556, 872
- Allard, F., Hauschildt, P. H., Alexander, D. R., Tamanai, A., & Schweitzer, A. 2001, *ApJ*, 556, 357
- Allen, P. R. 2007, *ApJ*, 668, 492

- Allen, P. R., Koerner, D. W., McElwain, M. W., Cruz, K. L., & Reid, I. N. 2007, *AJ*, 133, 971
- Apai, D., Radigan, J., Buenzli, E., et al. 2013, *ApJ*, 768, 121
- Artigau, E., Bouchard, S., Doyon, R., & Lafreniere, D. 2009, *ApJ*, 701, 1534
- Bailer-Jones, C. A. L. 2004, *A&A*, 419, 703
- Bouy, H., Martin, E. L., Brandner, W., & Bouvier, J. 2005, *AJ*, 129, 511
- Bouy, H., Duchêne, G., Köhler, R., et al. 2004, *A&A*, 423, 341
- Bowler, B. P., Liu, M. C., & Dupuy, T. J. 2010, *ApJ*, 710, 45
- Buenzli, E., Apai, D., Morley, C. V., et al. 2012, *ApJL*, 760, L31
- Burgasser, A. J. 2004, *ApJS*, 155, 191
- . 2007, *ApJ*, 659, 655
- Burgasser, A. J., Cruz, K. L., Cushing, M., et al. 2010, *ApJ*, 710, 1142
- Burgasser, A. J., Geballe, T. R., Leggett, S. K., Kirkpatrick, J. D., & Golimowski, D. A. 2006, *ApJ*, 637, 1067
- Burgasser, A. J., Kirkpatrick, J. D., McElwain, M. W., et al. 2003, *AJ*, 125, 850
- Burgasser, A. J., McElwain, M. W., Kirkpatrick, J. D., et al. 2004, *AJ*, 127, 2856
- Burgasser, A. J., Reid, I. N., Leggett, S. K., et al. 2005, *ApJ*, 634, L177
- Burgasser, A. J., Cushing, M. C., Kirkpatrick, J. D., et al. 2011, *ApJ*, 735, 116
- Burningham, B., Pinfield, D. J., Lucas, P. W., et al. 2010, *MNRAS*, 406, 1885
- Burrows, A., Sudarsky, D., & Hubeny, I. 2006, *ApJ*, 640, 1063
- Casali, M., Adamson, A., Alves de Oliveira, C., et al. 2007, *A&A*, 467, 777
- Chiu, K., Fan, X., Leggett, S. K., et al. 2006, *AJ*, 131, 2722
- Cross, N. J. G., Collins, R. S., Mann, R. G., et al. 2012, *A&A*, 548, 119
- Cruz, K. L., Reid, I. N., Liebert, J., Kirkpatrick, J. D., & Lowrance, P. J. 2003, *AJ*, 126, 2421
- Cruz, K. L., Reid, I. N., Kirkpatrick, J. D., et al. 2007, *AJ*, 133, 439
- Cushing, M. C., Rayner, J. T., & Vacca, W. D. 2005, *ApJ*, 623, 1115
- Cushing, M. C., Vacca, W. D., & Rayner, J. T. 2004, *PASP*, 116, 362

- Cushing, M. C., Kirkpatrick, J. D., Gelino, C. R., et al. 2011, *ApJ*, 743, 50
- Cutri, R. M., Wright, E. L., Conrow, T., et al. 2012, Explanatory Supplement to the WISE All-Sky Data Release Products
- Day-Jones, A. C., Marocco, F., Pinfield, D. J., et al. 2013, *MNRAS*, 430, 1171
- Deacon, N. R., Liu, M. C., Magnier, E. A., et al. 2011, *AJ*, 142, 77
- Dupuy, T. J., & Liu, M. C. 2012, *ApJS*, 201, 19
- Dupuy, T. J., Liu, M. C., Bowler, B. P., et al. 2010, *ApJ*, 721, 1725
- Dupuy, T. J., Liu, M. C., & Ireland, M. J. 2009, *ApJ*, 699, 168
- Enoch, M. L., Brown, M. E., & Burgasser, A. J. 2003, *AJ*, 126, 1006
- Epchtein, N., Deul, E., Derriere, S., et al. 1999, *A&A*, 349, 236
- Geballe, T. R., Knapp, G. R., Leggett, S. K., et al. 2002, *ApJ*, 564, 466
- Geißler, K., Metchev, S., Kirkpatrick, J. D., Berriman, G. B., & Looper, D. L. 2011, *ApJ*, 732, 56
- Gelino, C. R., Kirkpatrick, J. D., Cushing, M. C., et al. 2011, *AJ*, 142, 57
- Gliese, W., & Jahreiss, H. 1995, *VizieR On-line Data Catalog: V/70A*. Originally published in: *Astron. Rechen-Institut*, 5070, 0
- Goldman, B., Cushing, M. C., Marley, M. S., et al. 2008, *A&A*, 487, 277
- Golimowski, D. A., Leggett, S. K., Marley, M. S., et al. 2004, *AJ*, 127, 3516
- Hambly, N. C., Collins, R. S., Cross, N. J. G., et al. 2008, *MNRAS*, 384, 637
- Hewett, P. C., Warren, S. J., Leggett, S. K., & Hodgkin, S. T. 2006, *MNRAS*, 367, 454
- Hodgkin, S. T., Irwin, M. J., Hewett, P. C., & Warren, S. J. 2009, *MNRAS*, 394, 675
- Irwin, M. J., Lewis, J., Hodgkin, S., et al. 2004, *Optimizing Scientific Return for Astronomy through Information Technologies*. Edited by Quinn, 5493, 411
- Kaiser, N., Burgett, W., Chambers, K., et al. 2010, *Ground-based and Airborne Telescopes III*. Edited by Stepp, 7733, 12
- Khandrika, H., Burgasser, A. J., Melis, C., et al. 2013, *AJ*, 145, 71
- Kirkpatrick, J. D. 2005, *ARAA*, 43, 195
- Kirkpatrick, J. D., Reid, I. N., Liebert, J., et al. 1999, *ApJ*, 519, 802

- Kirkpatrick, J. D., Looper, D. L., Burgasser, A. J., et al. 2010, *ApJS*, 190, 100
- Kirkpatrick, J. D., Cushing, M. C., Gelino, C. R., et al. 2011, *ApJS*, 197, 19
- Kirkpatrick, J. D., Gelino, C. R., Cushing, M. C., et al. 2012, *ApJ*, 753, 156
- Knapp, G. R., Leggett, S. K., Fan, X., et al. 2004, *AJ*, 127, 3553
- Koen, C., Tanabé, T., Tamura, M., & Kusakabe, N. 2005, *MNRAS*, 362, 727
- Konopacky, Q. M., Ghez, A. M., Barman, T. S., et al. 2010, *ApJ*, 711, 1087
- Lawrence, A., Warren, S. J., Almaini, O., et al. 2007, *MNRAS*, 379, 1599
- . 2012, *VizieR On-line Data Catalog*, 2314, 0
- Leggett, S. K., Geballe, T. R., Fan, X., et al. 2000, *ApJ*, 536, L35
- Leggett, S. K., Burningham, B., Saumon, D., et al. 2010, *ApJ*, 710, 1627
- Liu, M. C., Dupuy, T. J., & Ireland, M. J. 2008, *ApJ*, 689, 436
- Liu, M. C., Dupuy, T. J., & Leggett, S. K. 2010, *ApJ*, 722, 311
- Liu, M. C., Leggett, S. K., Golimowski, D. A., et al. 2006, *ApJ*, 647, 1393
- Liu, M. C., Deacon, N. R., Magnier, E. A., et al. 2011a, *ApJL*, 740, L32
- Liu, M. C., Delorme, P., Dupuy, T. J., et al. 2011b, *ApJ*, 740, 108
- Lodieu, N., Burningham, B., Day-Jones, A., et al. 2012, *A&A*, 548, 53
- Looper, D. L., Gelino, C. R., Burgasser, A. J., & Kirkpatrick, J. D. 2008, *ApJ*, 685, 1183
- Luhman, K. L., Burgasser, A. J., & Bochanski, J. J. 2011, *ApJL*, 730, L9
- Mace, G. N., Kirkpatrick, J. D., Cushing, M. C., et al. 2013, *ApJS*, 205, 6
- Magnier, E. 2006, *The Advanced Maui Optical and Space Surveillance Technologies Conference*, 50
- Magnier, E. 2007, in *ASP Conf. Ser.*, 364, *The Future of Photometric, Spectrophotometric and Polarimetric Standardization*, ed. C. Sterken, San Francisco, CA, 153
- Magnier, E. A., Liu, M., Monet, D. G., & Chambers, K. C. 2008, in *IAU 248, 2007*, 553–559
- Marley, M. S., Saumon, D., & Goldblatt, C. 2010, *ApJL*, 723, L117
- Martín, E. L., Delfosse, X., Basri, G., et al. 1999, *AJ*, 118, 2466

- Metchev, S. A., Kirkpatrick, J. D., Berriman, G. B., & Looper, D. L. 2008, *ApJ*, 676, 1281
- Nakajima, T., Oppenheimer, B. R., Kulkarni, S. R., et al. 1995, *Nature*, 378, 463
- Radigan, J., Jayawardhana, R., Lafreniere, D., et al. 2012, *ApJ*, 750, 105
- Rayner, J. T., Toomey, D. W., Onaka, P. M., et al. 2003, *PASP*, 115, 362
- Reid, I. N., Cruz, K. L., Kirkpatrick, J. D., et al. 2008, *AJ*, 136, 1290
- Reid, I. N., Gizis, J. E., & Hawley, S. L. 2002, *AJ*, 124, 2721
- Reiners, A., & Basri, G. 2008, *ApJ*, 684, 1390
- Rockenfeller, B., Bailer-Jones, C. A. L., & Mundt, R. 2006, *A&A*, 448, 1111
- Saumon, D., & Marley, M. S. 2008, *ApJ*, 689, 1327
- Skrutskie, M. F., Cutri, R. M., Stiening, R., et al. 2006, *AJ*, 131, 1163
- Stephens, D. C., & Leggett, S. K. 2004, *PASP*, 116, 9
- Stephens, D. C., Leggett, S. K., Cushing, M. C., et al. 2009, *ApJ*, 702, 154
- Tinney, C. G., Burgasser, A. J., & Kirkpatrick, J. D. 2003, *AJ*, 126, 975
- Tokunaga, A. T., Simons, D. A., & Vacca, W. D. 2002, *PASP*, 114, 180
- Tonry, J. L., Stubbs, C. W., Lykke, K. R., et al. 2012, *ApJ*, 750, 99
- Tsuji, T. 2005, *ApJ*, 621, 1033
- Vacca, W. D., Cushing, M. C., & Rayner, J. T. 2003, *PASP*, 115, 389
- West, A. A., Morgan, D. P., Bochanski, J. J., et al. 2011, *AJ*, 141, 97
- Wright, E. L., Eisenhardt, P. R. M., Mainzer, A. K., et al. 2010, *AJ*, 140, 1868
- York, D. G., Adelman, J., Anderson, J. E. J., et al. 2000, *AJ*, 120, 1579

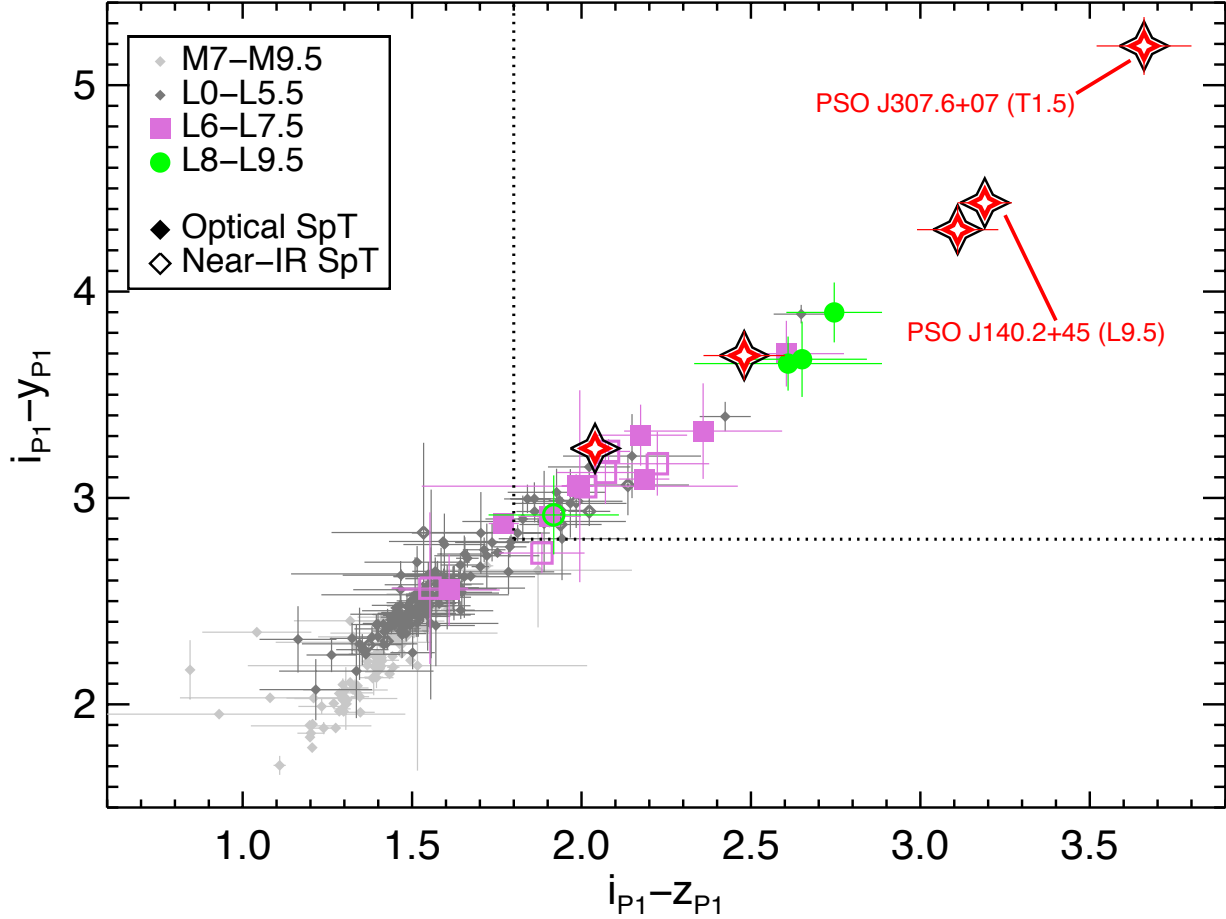


Fig. 1.— $i_{P1}-z_{P1}$ vs. $i_{P1}-y_{P1}$ diagram for known ultracool dwarfs. Late-L dwarfs are indicated with magenta squares (types L6–L7.5) and green circles (L8–L9.5); no known T dwarfs have i_{P1} detections in our PS1+*WISE* database. Objects with optical spectral types are plotted with filled symbols, and objects with near-infrared spectral types are plotted with open symbols. The dotted black lines indicate the color cuts used in our search; we selected objects above and to the right of the dotted lines, but only enforced each cut for objects which had $\sigma < 0.2$ mag and at least two detections in both bands. Our newly identified objects are marked with large red four-point stars, with the spectroscopic variable candidates labeled individually. (Two of our discoveries and many known L dwarfs were also not detected in i_{P1} .) The new discoveries clearly extend the linear $i_{P1}-z_{P1}$ vs. $i_{P1}-y_{P1}$ locus to redder colors.

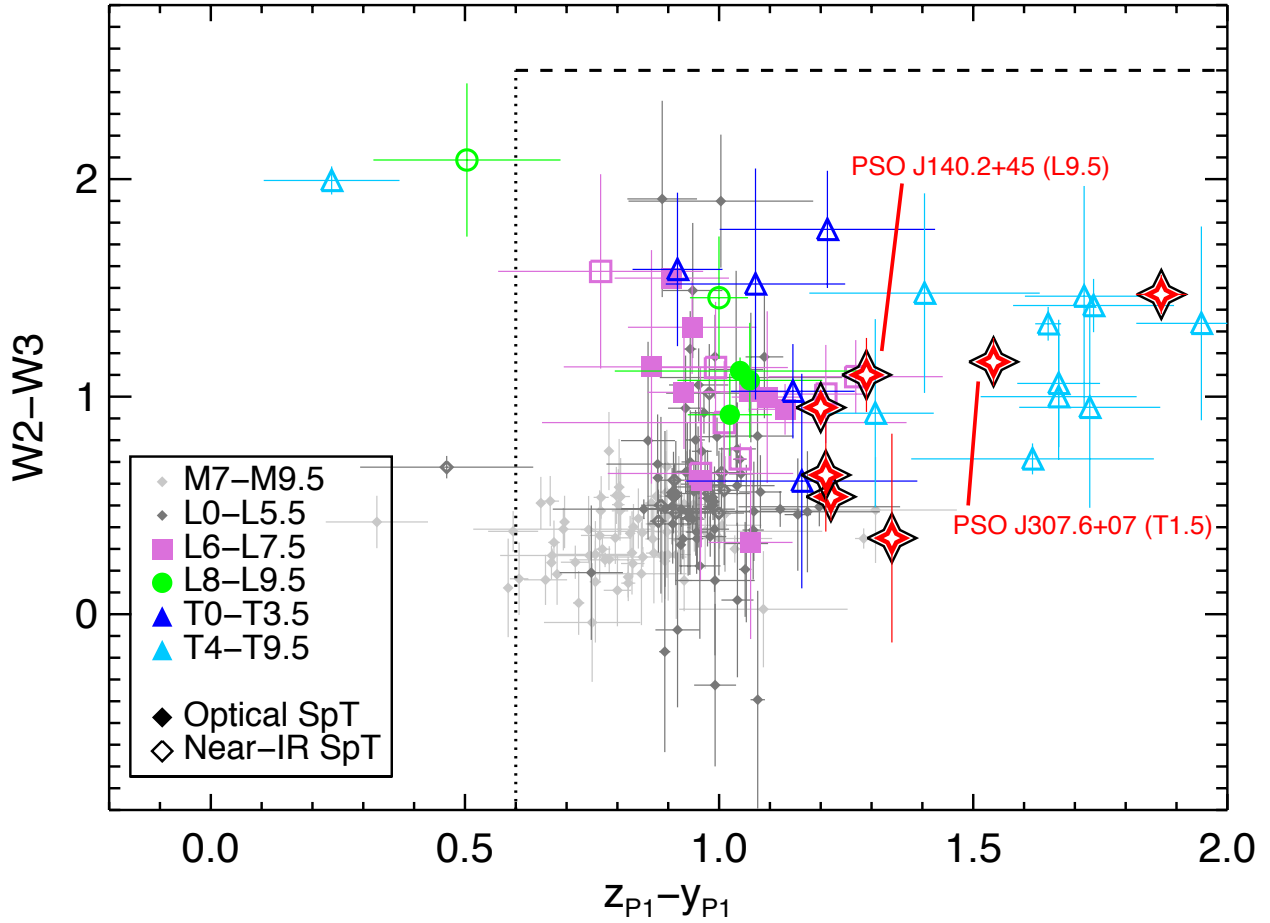


Fig. 2.— $W2 - W3$ vs. $z_{P1} - y_{P1}$ diagram for known ultracool dwarfs, using the same colors and symbols as Figure 1; in addition, early-T dwarfs are indicated by dark blue triangles, and mid- and late-T dwarfs by light blue triangles. The vertical dotted line indicates our $z_{P1} - y_{P1}$ cut, which we applied only to objects with $\sigma_z < 0.2$ mag and at least two z_{P1} detections. The horizontal dashed line represents our $W2 - W3$ cut, which we applied to all objects in our search. We selected objects below and to the right of these lines.

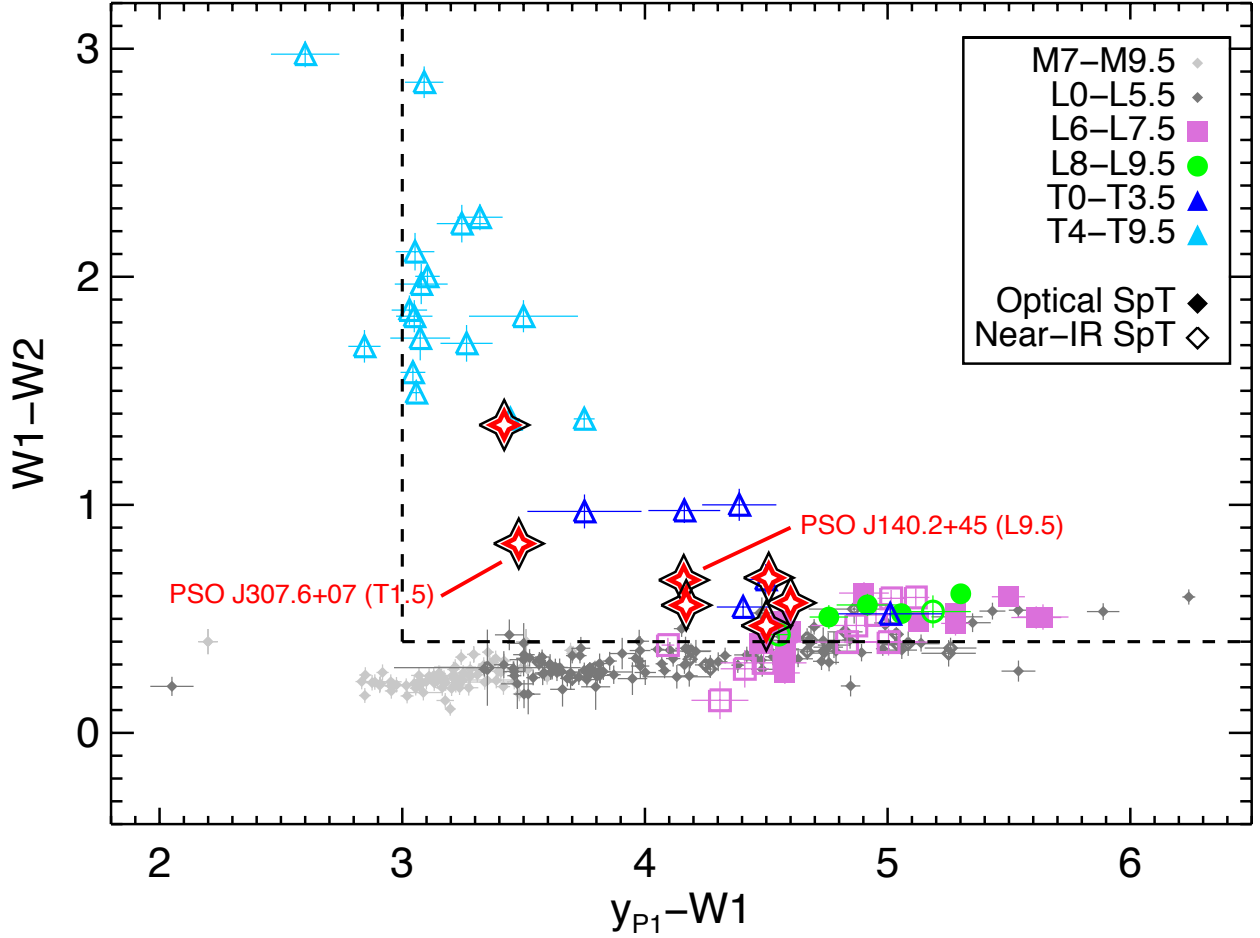


Fig. 3.— $W1 - W2$ vs. $y_{P1} - W1$ diagram for known ultracool dwarfs, using the same colors, lines and symbols as Figures 1 and 2. We selected objects with colors above and to the right of the dashed lines. All of our discoveries lie in the typical region of this color space for late-L and early-T dwarfs, except that PSO J307.6+07 is fairly blue in $y_{P1} - W1$ for an early-T dwarf.

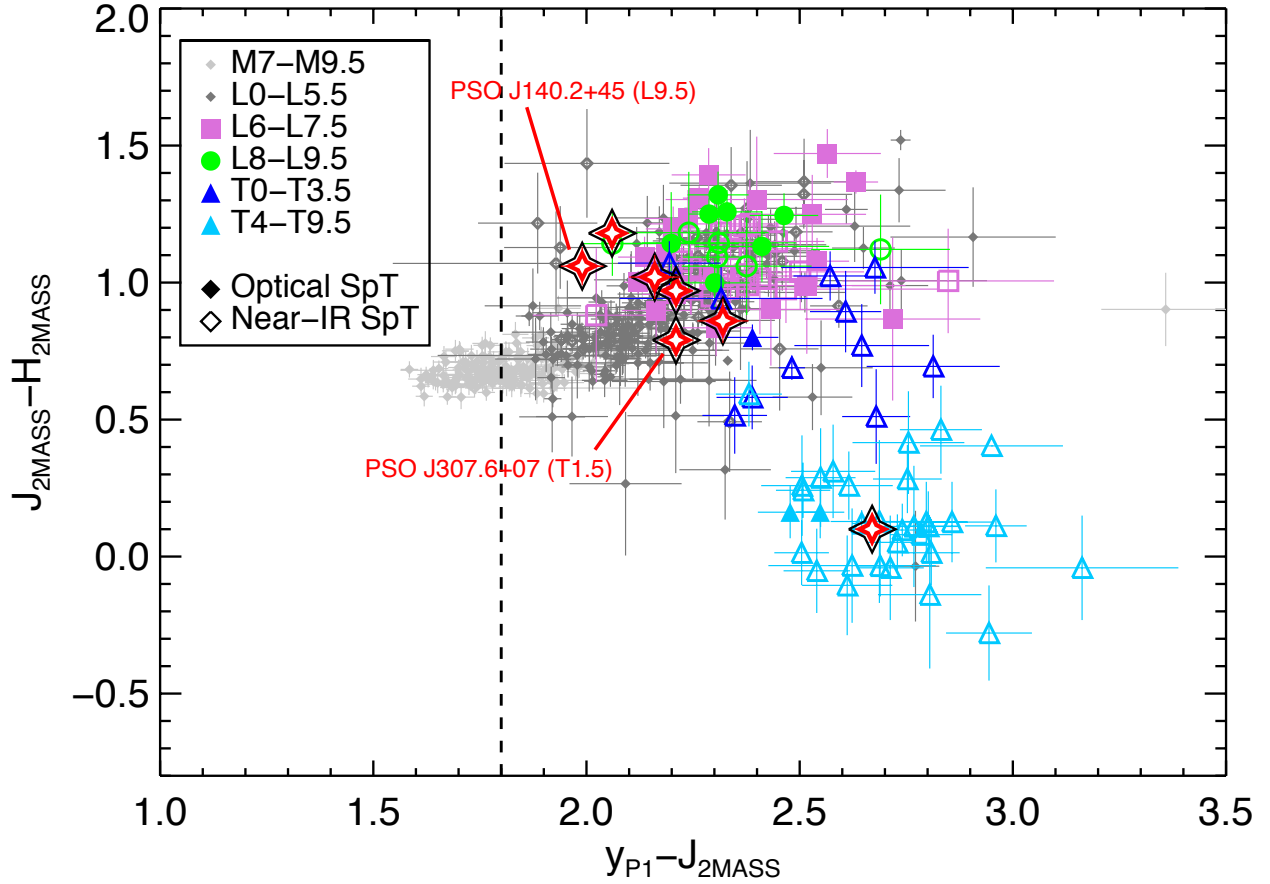


Fig. 4.— $J_{2MASS} - H_{2MASS}$ vs. $y_{P1} - J_{2MASS}$ diagram for known ultracool dwarfs, using the same colors, lines and symbols as Figures 1 and 2. We selected objects to the right of the dashed line. The red object at lower right is the T5 PSO J339.0+51; the other red objects have spectral types L9–T1. PSO J339.0+51 has typical $J_{2MASS} - H_{2MASS}$ and $y_{P1} - J_{2MASS}$ values for its spectral type, while all of our other new discoveries are blue in $y_{P1} - J_{2MASS}$ compared to known late-L and early-T dwarfs, possibly because previous searches have tended to find redder objects.

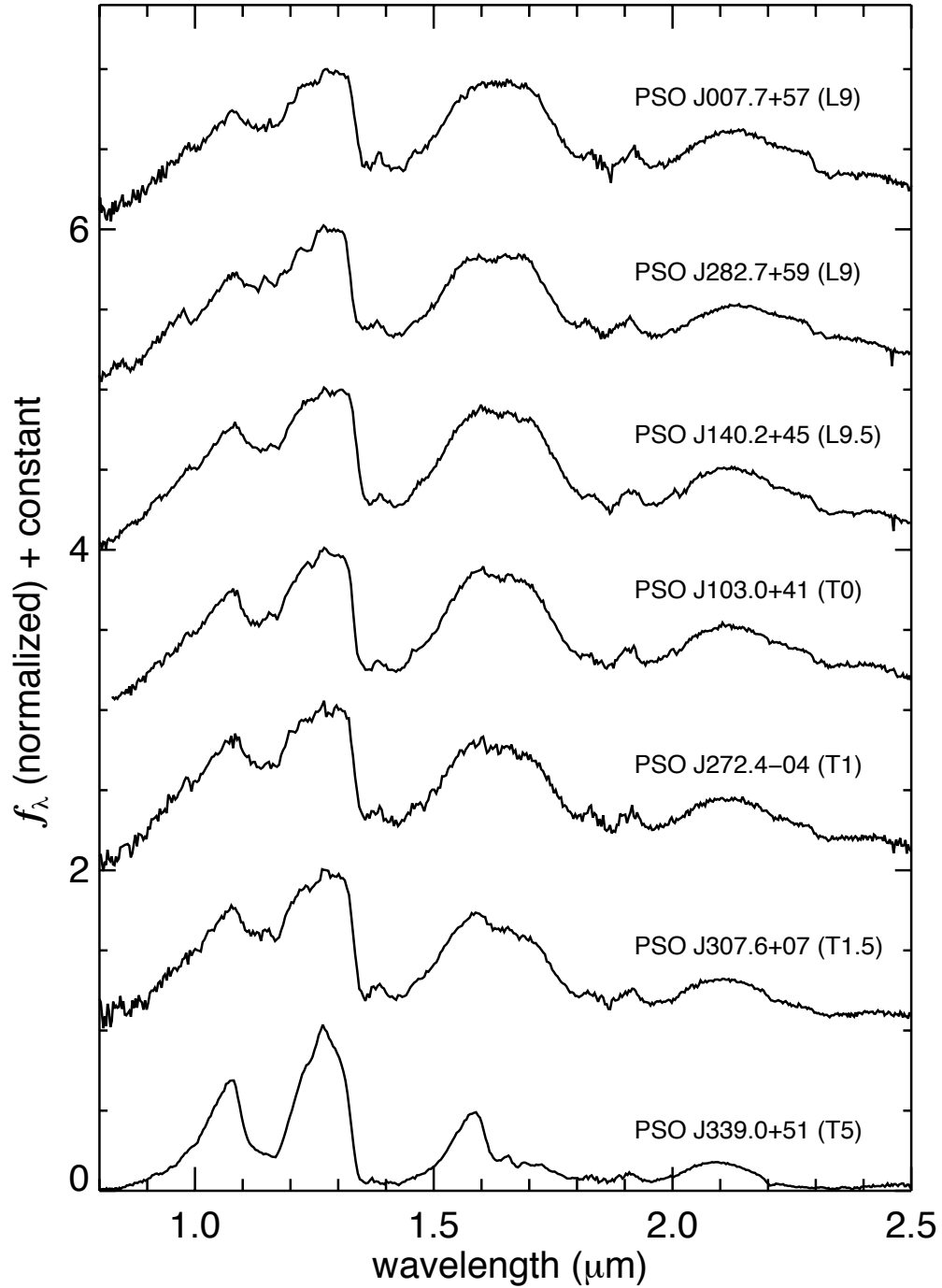


Fig. 5.— SpeX prism spectra for our seven objects, normalized at the J -band peak ($1.27\ \mu\text{m}$), arranged from earliest to latest spectral type and offset by a constant. Spectral typing was done by visual comparison with the near-infrared standards defined by Burgasser et al. (2006) and Kirkpatrick et al. (2010).

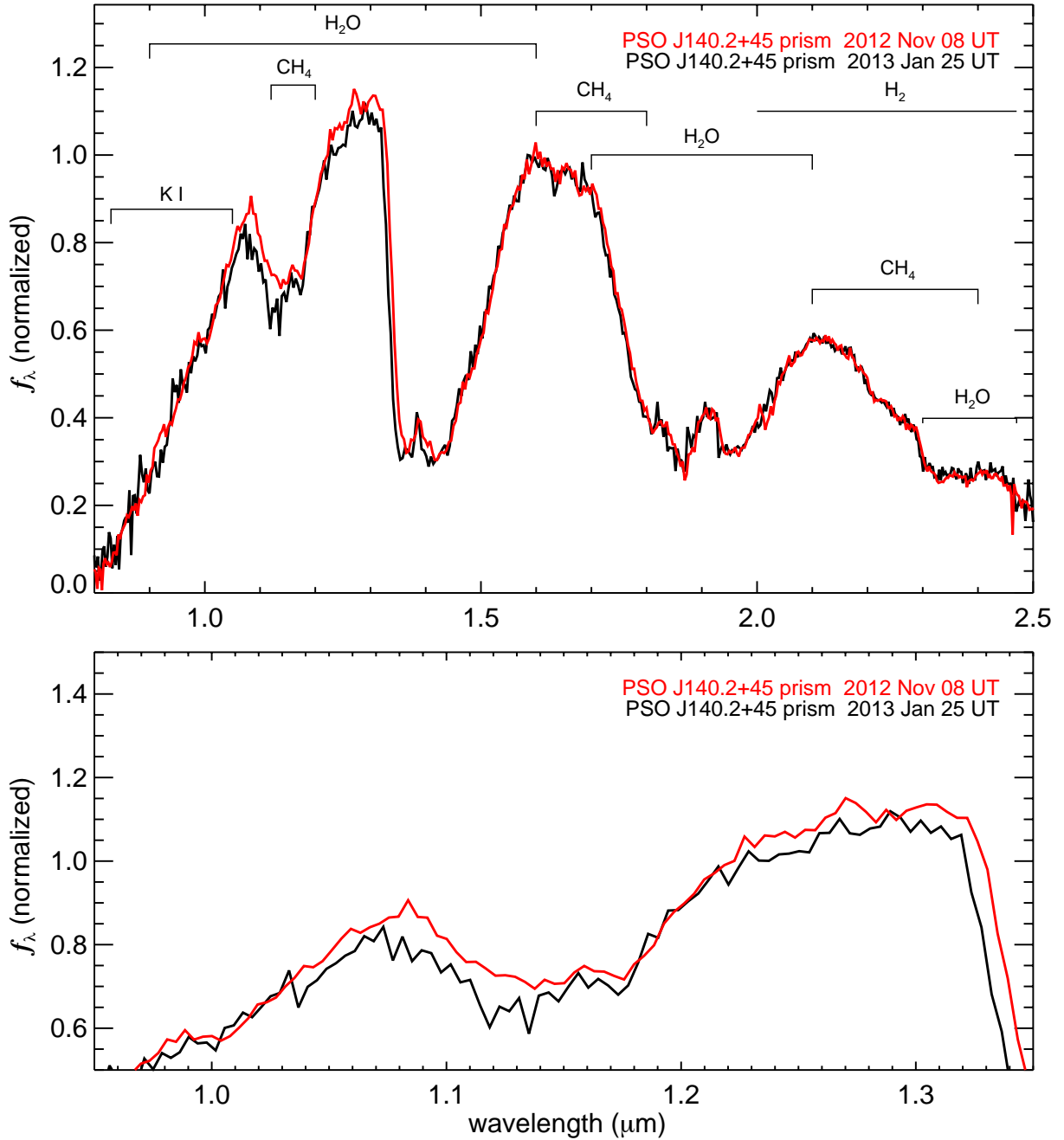


Fig. 6.— *Top*: Prism spectra ($R \sim 100$) for PSO J140.2+45 taken in November 2012 (black) and January 2013 (red), both with SpeX on IRTF. *Bottom*: Same as top window, but showing only the Y- and J-bands. The changes in flux in the Y-band peak (1.06 – 1.10 μm) and marginally in the J-band (1.16 – 1.33 μm) suggest variability similar to that previously detected in two other early-T dwarfs (Artigau et al. 2009; Radigan et al. 2012; Apai et al. 2013). The spectra have been normalized to the H-band peak (1.58 μm) to highlight the Y- and J-band variations.

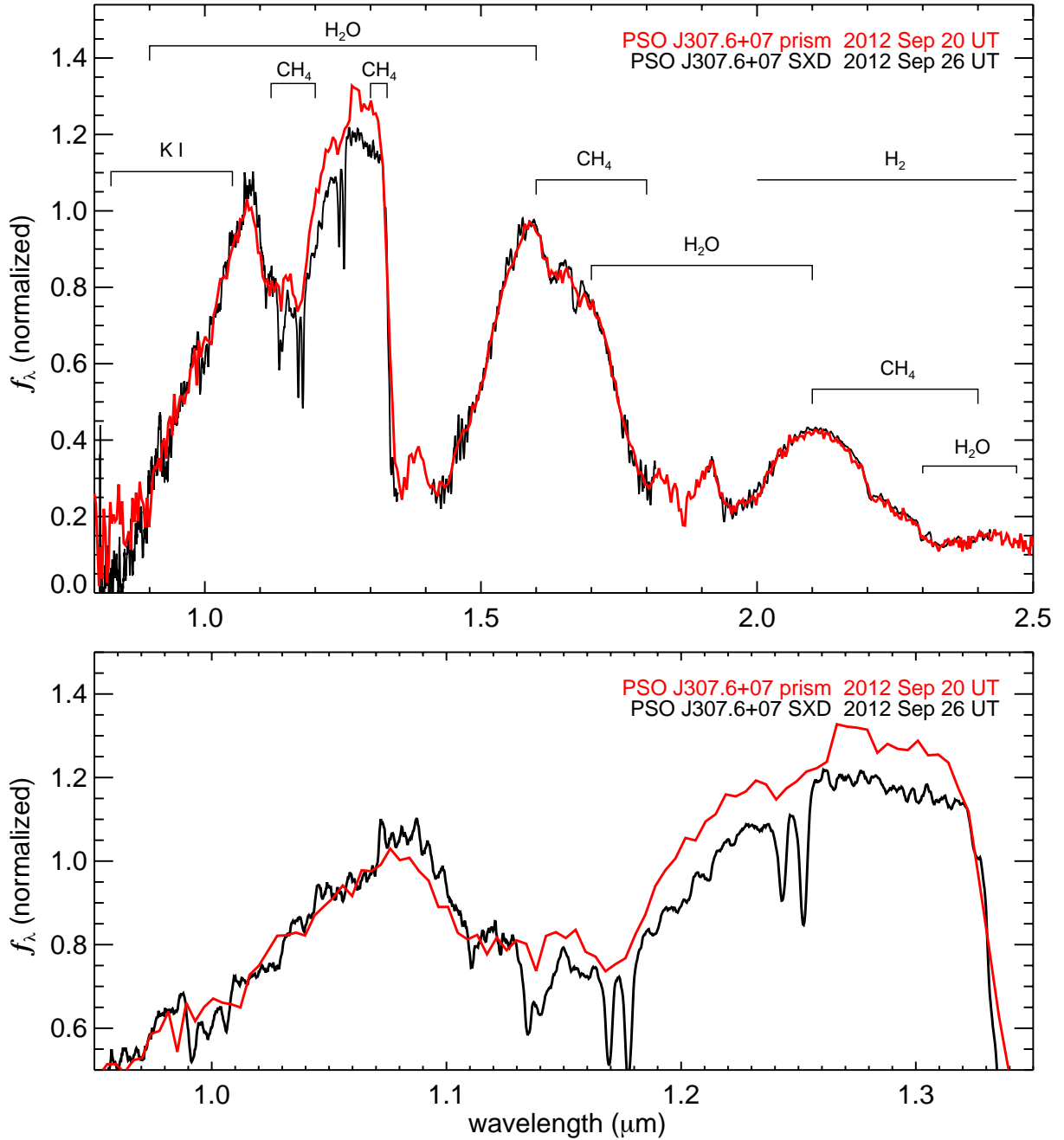


Fig. 7.— *Top:* Spectra for PSO J307.6+07 taken six nights apart, both with SpeX on IRTF. The prism spectrum (red) has $R \sim 100$ while the SXD spectrum (black) has $R \sim 750$ and is smoothed by an 8-pixel box. *Bottom:* Same as top window, but showing only the Y- and J-bands. The change in flux in the J-band (1.16 – 1.33 μm) clearly suggests variability. The slight difference visible in the Y-band (1.00 – 1.13 μm) flux is not statistically significant. The spectra have been normalized to the H-band peak (1.58 μm) to highlight the J-band variation.

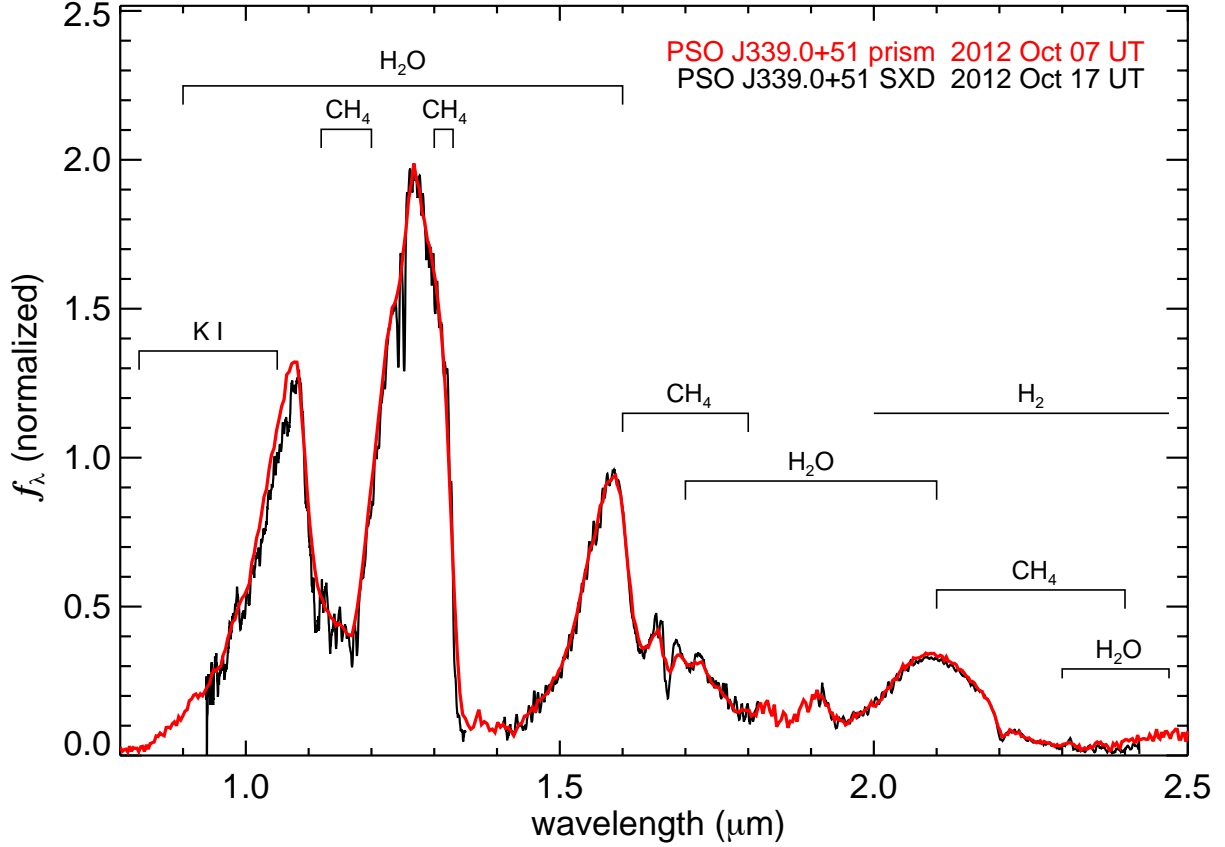


Fig. 8.— Spectra for PSO J339.0+51 taken ten nights apart, both with SpeX on IRTF. The prism spectrum (red) has $R \sim 100$ while the SXD spectrum (black) has $R \sim 750$ and is smoothed by an 8-pixel box. No clear sign of variability is seen between these two spectra; the slight difference visible in the Y -band ($1.00 - 1.13 \mu\text{m}$) flux is not statistically significant. As in Figures 6 and 7, these spectra have been normalized to the H -band peak.

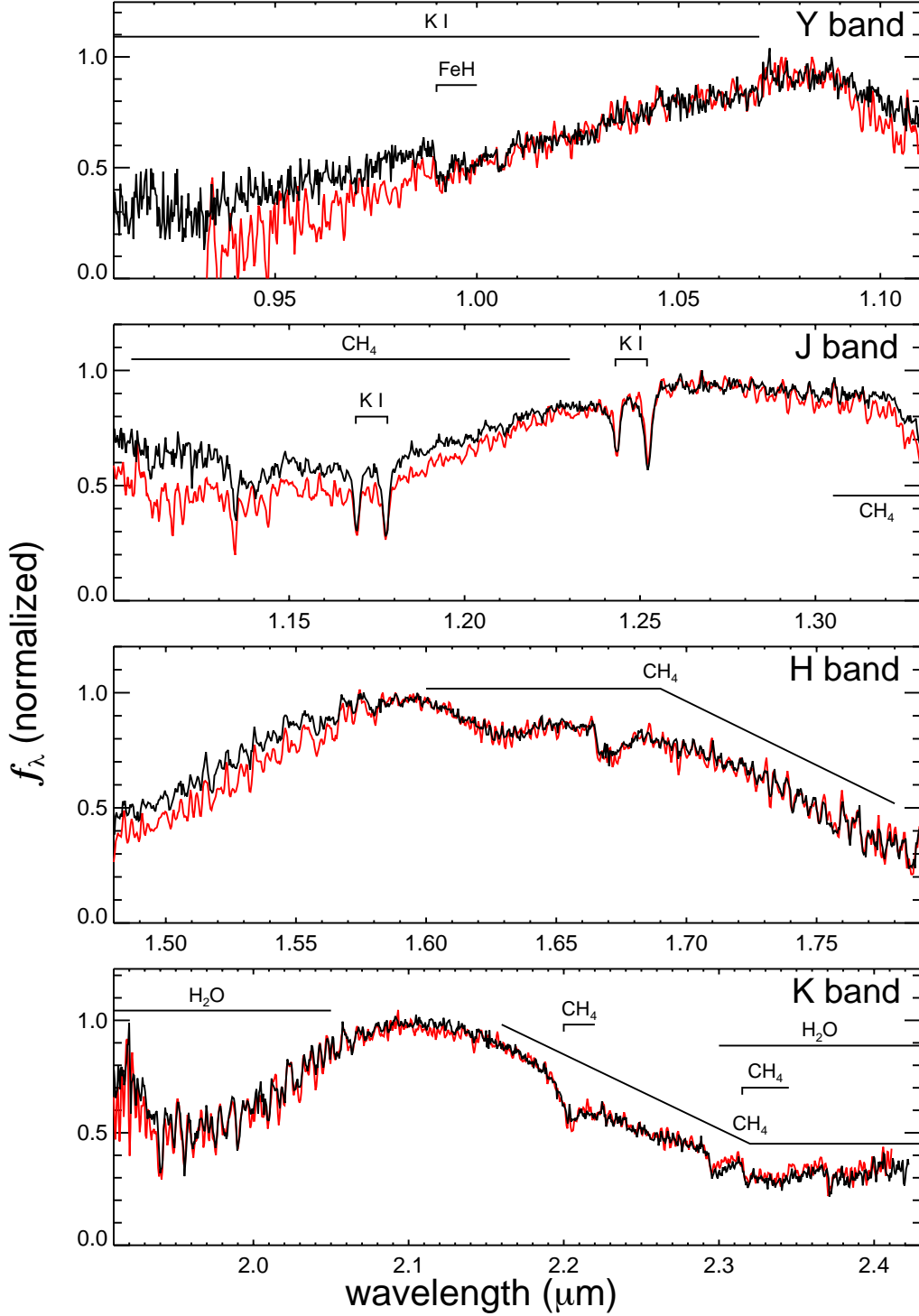


Fig. 9.— SpeX SXD spectra for PSO J307.6+07 (T1.5, black) and the T2 standard SDSS 1254–0122 (red, Cushing et al. 2005). The spectra are normalized to the peak value in each band and show the same prominent absorption features. The relative faintness of SDSS 1254–0122 in parts of the Y-, J- and H-bands is expected because PSO J307.6+07 is half a spectral type earlier.

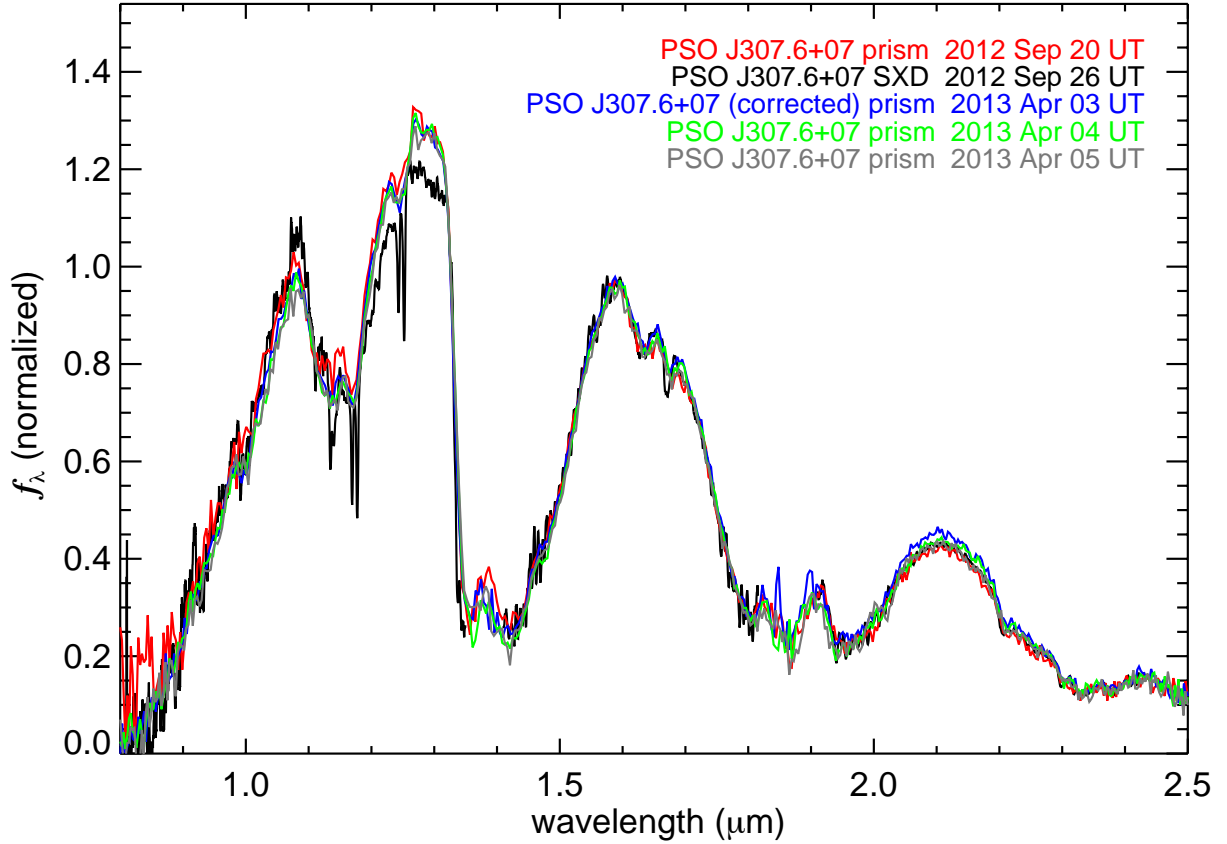


Fig. 10.— Spectra of PSO J307.6+07 taken in 2012 September (red and black, from Figure 7) and 2013 April (blue, green, and grey). The September 26 SXD spectrum (black) is smoothed by an 8-pixel box. The April 3 spectrum (blue) has been corrected for dimming seen in the comparison M1V star 2MASS J2041+0014 on that night. As in previous figures, these spectra have been normalized to the H -band peak. Unlike the September spectra, the April spectra show no variation. In the Y -band, both of the September spectra differ from the April spectra; in the J -band, only September 26 is different.

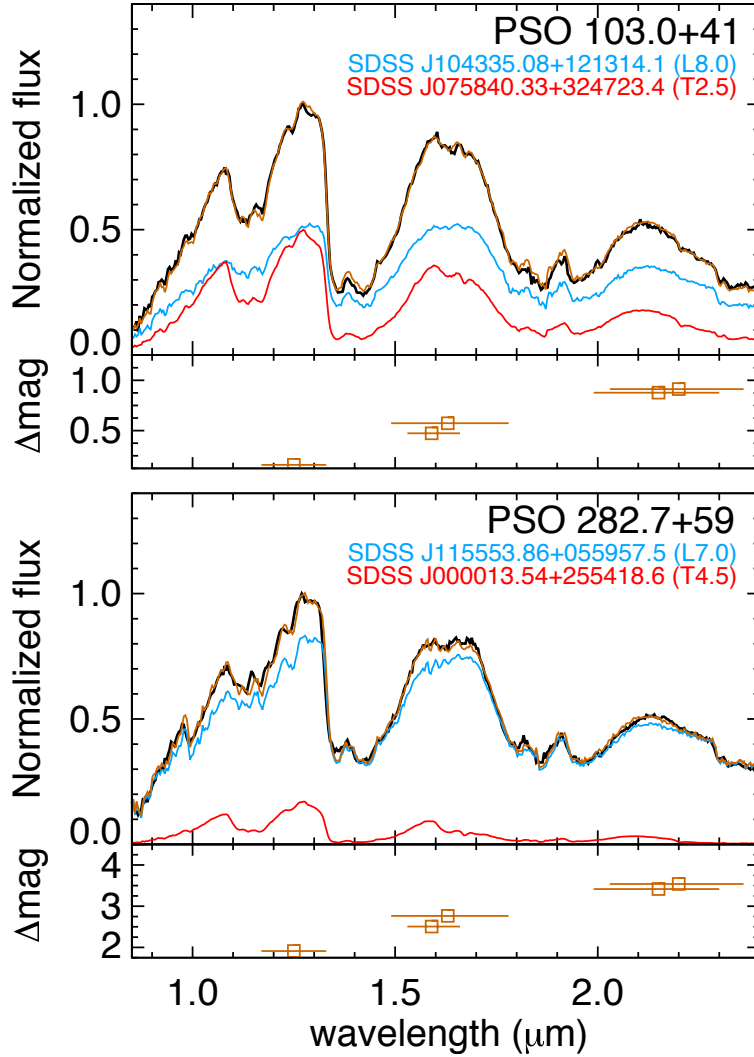


Fig. 11.— Best-matching template pairings for our candidate binaries PSO J103.0+41 (*top*) and PSO J282.7+59 (*bottom*). Observed spectra are shown in black, individual component templates in blue and red, and convolved templates in brown. The lower subpanels show the resulting flux ratios over standard NIR bandpasses computed from the best-matching template pairs (open brown squares).

Table 1. IRTF/SpeX Observations

Object	Date (UT)	Conditions	Seeing (arcsec)	Airmass	Mode	Slit (arcsec)	R ($\equiv \lambda/\Delta\lambda$)	T_{int} (s)	Standard
PSO J007.7921+57.8267	2012 Sep 24	Clear	0.9	1.27	prism	0.8×15	~ 100	200	HD 240290
PSO J103.0927+41.4601	2012 Sep 26	Clear	0.5	1.18	prism	0.5×15	~ 100	960	HD 39250
PSO J140.2308+45.6487	2012 Nov 8	Clear	0.8	1.32	prism	0.8×15	~ 100	720	HD 33654
PSO J140.2308+45.6487	2013 Jan 25	Clear	0.8	1.23	prism	0.8×15	~ 100	180	HD 79108
PSO J272.4689-04.8036	2012 Oct 14	Clear	1.1	1.28	prism	0.8×15	~ 100	720	HD 173591
PSO J282.7576+59.5858	2012 Sep 26	Clear	0.4	1.39	prism	0.8×15	~ 100	240	HD 240290
PSO J307.6784+07.8263	2012 Sep 20	Clear	0.6	1.15	prism	0.8×15	~ 100	80	HD 189920
PSO J307.6784+07.8263	2012 Sep 26	Clear	0.5	1.02	SXD	0.8×15	~ 750	1440	HD 189920
PSO J307.6784+07.8263	2013 Apr 03	Clear	1.0	1.43	prism	0.8×15	~ 100	180	HD 187170
PSO J307.6784+07.8263	2013 Apr 04	Clear	0.5	1.43	prism	0.8×15	~ 100	480	HD 187170
PSO J307.6784+07.8263	2013 Apr 05	Cloudy	0.8	1.50	prism	0.8×15	~ 100	320	HD 180150
PSO J339.0734+51.0978	2012 Oct 7	Cloudy	0.9	1.19	prism	0.8×15	~ 100	1200	HD 222749
PSO J339.0734+51.0978	2012 Oct 17	Cloudy	0.5	1.18	SXD	0.8×15	~ 750	1920	HD 209932

Table 2. Properties of New Discoveries

Property	PSO J007.7921+57.8267	PSO J103.0927+41.4601	PSO J140.2308+45.6487 ^a	PSO J272.4689–04.8036 ^b
Astrometry				
PS1 R.A. (J2000)	7.7921°	103.0927°	140.2308°	272.4689°
	00 ^h 31 ^m 10 ^s .11	06 ^h 52 ^m 22 ^s .25	09 ^h 20 ^m 55 ^s .40	18 ^h 09 ^m 52 ^s .53
PS1 Dec. (J2000)	+57.8267°	+41.4601°	+45.6487°	–4.8036°
	+57°49′36.3″	+41°27′36.2″	+45°38′55.3″	–04°48′13.0″
PS1 epoch	2011.410	2011.400	2011.483	2011.020
Galactic longitude	120.2261°	174.8199°	174.3678°	23.8612°
Galactic latitude	–4.9385°	17.7353°	44.7239°	6.9942°
$\mu_\alpha \cos \delta$ (mas yr ^{–1})	523 ± 17	–8 ± 6	–42 ± 23	–62 ± 18
μ_δ (mas yr ^{–1})	–1 ± 16	–38 ± 6	–843 ± 23	–429 ± 17
2MASS designation	J00310928+5749364	J06522224+4127366	J09205549+4539058	J18095256-0448081
2MASS epoch	1998.983	1998.268	1999.139	1998.747
WISE designation	J003110.04+574936.3	J065222.24+412736.1	J092055.40+453856.3	J180952.53-044812.5
WISE epoch	2010.316	2010.233	2010.307	2010.224
Photometry				
PS1 <i>z</i> (AB mag)	18.24 ± 0.01	18.85 ± 0.02	18.50 ± 0.01	18.80 ± 0.03
PS1 <i>y</i> (AB mag)	17.01 ± 0.01	17.64 ± 0.01	17.21 ± 0.01	17.46 ± 0.02
2MASS <i>J</i> (mag)	14.95 ± 0.04	15.48 ± 0.06	15.22 ± 0.05	15.14 ± 0.06
2MASS <i>H</i> (mag)	13.78 ± 0.04	14.46 ± 0.05	14.16 ± 0.05	14.28 ± 0.05
2MASS <i>K_s</i> (mag)	13.22 ± 0.03	13.89 ± 0.05	13.73 ± 0.05	13.96 ± 0.06
MKO <i>Y</i> (mag)
MKO <i>J</i> (mag)	14.79 ± 0.01 ^c	15.36 ± 0.01 ^c	15.04 ± 0.01 ^c	15.15 ± 0.01 ^d
MKO <i>H</i> (mag)	...	14.51 ± 0.03 ^c	14.19 ± 0.02 ^c	...
MKO <i>K</i> (mag)	...	13.95 ± 0.03 ^c	13.77 ± 0.01 ^c	13.98 ± 0.01 ^{d,e}
WISE <i>W1</i> (mag)	12.41 ± 0.02	13.13 ± 0.02	13.06 ± 0.02	13.29 ± 0.03
WISE <i>W2</i> (mag)	11.84 ± 0.02	12.44 ± 0.03	12.39 ± 0.03	12.73 ± 0.03
WISE <i>W3</i> (mag)	11.30 ± 0.10	11.80 ± 0.25	11.28 ± 0.17	12.38 ± 0.47
Spectral Indices				
H ₂ O- <i>J</i>	0.659 (L8.5)	0.588 (T0.4)	0.647 (L8.9)	0.657 (L8.6)
CH ₄ - <i>J</i>	0.835 (<T0)	0.709 (<T0)	0.875 (<T0)	0.773 (<T0)
H ₂ O- <i>H</i>	0.665 (L7.8)	0.575 (T0.6)	0.608 (L9.7)	0.630 (L9.0)
CH ₄ - <i>H</i>	1.047 (<T1)	0.981 (T1.1)	1.002 (<T1)	0.972 (T1.1)
CH ₄ - <i>K</i>	0.844 (L8.7)	0.778 (L9.9)	0.749 (T0.3)	0.719 (T0.7)
H ₂ O- <i>K</i>	0.687 (—)	0.658 (—)	0.631 (—)	0.644 (—)
Physical Properties				
Near-IR spectral type	L9	T0	L9.5	T1
Photometric distance (pc)	11.6 ± 1.0	14.2 ± 1.2	14.3 ± 1.2	15.0 ± 1.3
v_{tan} (km s ^{–1})	29 ± 3	3 ± 1	57 ± 5	31 ± 3

Table 2—Continued

Property	PSO J007.7921+57.8267	PSO J103.0927+41.4601	PSO J140.2308+45.6487 ^a	PSO J272.4689–04.8036 ^b
Distinctive feature	—	Possible binary	<i>J</i> -band variable	Possible variable

^aFirst identified photometrically by Aberasturi et al. (2011); also identified and spectrally typed by Mace et al. (2013).

^bDiscovered independently by Mace et al. (2013).

^cPhotometry obtained with UKIRT/WFCAM on 2012 December 13–14 UT.

^dPhotometry obtained from the VISTA VHS catalog (Cross et al. 2012).

^eVISTA uses a K_s filter similar to 2MASS.

Table 3. Properties of New Discoveries

Property	PSO J282.7576+59.5858	PSO J307.6784+07.8263 ^a	PSO J339.0734+51.0978 ^a
Astrometry			
PS1 R.A. (J2000)	282.7576° 18 ^h 51 ^m 01 ^s .84	307.6784° 20 ^h 30 ^m 42 ^s .81	339.0734° 22 ^h 36 ^m 17 ^s .63
PS1 Dec. (J2000)	+59.5858° +59°35′08.9″	+7.8263° +07°49′34.6″	+51.0978° +51°05′52.0″
PS1 epoch	2011.177	2010.757	2010.688
Galactic longitude	89.5093°	51.9998°	102.3625°
Galactic latitude	23.2059°	−17.9389°	−6.2959°
$\mu_\alpha \cos \delta$ (mas yr ^{−1})	23 ± 19	659 ± 8	736 ± 14
μ_δ (mas yr ^{−1})	412 ± 19	−113 ± 9	330 ± 8
2MASS designation	J18510178+5935040	J20304235+0749358	J22361685+5105487
2MASS epoch	1999.432	2000.442	2000.760
WISE designation	J185101.83+593508.6	J203042.79+074934.7	J223617.59+510551.9
WISE epoch	2010.344	2010.333	2010.498
Photometry			
PS1 <i>z</i> (AB mag)	18.35 ± 0.01	17.97 ± 0.01	19.13 ± 0.05
PS1 <i>y</i> (AB mag)	17.15 ± 0.02	16.44 ± 0.01	17.25 ± 0.01
2MASS <i>J</i> (mag)	14.94 ± 0.04	14.23 ± 0.03	14.58 ± 0.04
2MASS <i>H</i> (mag)	13.97 ± 0.04	13.44 ± 0.03	14.49 ± 0.05
2MASS <i>K_s</i> (mag)	13.46 ± 0.05	13.32 ± 0.04	14.45 ± 0.09
MKO <i>Y</i> (mag)	...	15.22 ± 0.01 ^b	15.66 ± 0.01 ^b
MKO <i>J</i> (mag)	14.85 ± 0.01 ^b	14.05 ± 0.01 ^b	14.46 ± 0.01 ^b
MKO <i>H</i> (mag)	14.03 ± 0.02 ^b	13.48 ± 0.01 ^b	14.62 ± 0.02 ^b
MKO <i>K</i> (mag)
WISE <i>W1</i> (mag)	12.65 ± 0.02	12.96 ± 0.03	13.84 ± 0.03
WISE <i>W2</i> (mag)	12.18 ± 0.02	12.12 ± 0.03	12.48 ± 0.03
WISE <i>W3</i> (mag)	11.23 ± 0.07	10.96 ± 0.11	11.02 ± 0.08
Spectral Indices			
H ₂ O- <i>J</i>	0.678 (L8.0)	0.625 (L9.4)	0.225 (T5.1)
CH ₄ - <i>J</i>	0.652 (T0.1)	0.698 (<T0)	0.405 (T5.0)
H ₂ O- <i>H</i>	0.650 (L8.3)	0.586 (T0.4)	0.335 (T5.1)
CH ₄ - <i>H</i>	1.016 (<T1)	0.878 (T1.7)	0.410 (T5.2)
CH ₄ - <i>K</i>	0.897 (L7.5)	0.548 (T2.2)	0.203 (T5.3)
H ₂ O- <i>K</i>	0.705 (—)	0.579 (—)	0.443 (—)
Physical Properties			
Near-IR spectral type	L9	T1.5	T5
Photometric distance (pc)	13.5 ± 1.1	10.9 ± 0.9	9.4 ± 0.8
v_{tan} (km s ^{−1})	26 ± 3	35 ± 3	36 ± 3

Table 3—Continued

Property	PSO J282.7576+59.5858	PSO J307.6784+07.8263 ^a	PSO J339.0734+51.0978 ^a
Distinctive feature	Possible binary	<i>J</i> -band variable	Possible variable

^aDiscovered independently by Mace et al. (2013).

^bPhotometry obtained with UKIRT/WFCAM on 2012 September 19–21 UT.

Table 4. Properties of Candidate Binaries

Property	PSO J103.0927+41.4601	PSO J282.7576+59.5858
Primary Spectral Type	L8±1	L7±1
Secondary Spectral Type	T2.5±0.5	T4.5±1
ΔJ (2MASS mag)	0.24 ± 0.05	2.53 ± 0.78
ΔH (2MASS mag)	0.57 ± 0.05	3.04 ± 1.03
ΔK (2MASS mag)	0.91 ± 0.08	2.31 ± 0.65
ΔJ (MKO mag)	0.18 ± 0.05	1.81 ± 0.37
ΔH (MKO mag)	0.58 ± 0.04	2.53 ± 0.77
$\Delta \text{CH}_4\text{s}$ (MKO mag)	0.48 ± 0.04	3.13 ± 1.08
ΔK (MKO mag)	0.95 ± 0.09	1.90 ± 0.41

Note. — These spectral types and flux ratios are estimated from spectral decomposition. They have not been directly measured.